THE DEVELOPMENT OF A DUAL FREQUENCY EVENT TIMER

C.A. Steggerda
Department of Physics and Astronomy
University of Maryland
College Park, Maryland 20742

Telephone (301) 454 3406
Telex 908787

ABSTRACT

The fundamental concepts and equations of the Event Timer are discussed. The evolution of the Event Timer since the Herstmonceux conference and the specifications are stated. New circuits are described which reduce the RMS jitter to the range of 15 picoseconds. Under ideal conditions, over a period of one hour, the stability and the RMS variation of 1000 point mean points is in the order of one picosecond. Plans for a 5 picosecond resolution Timer are presented.

INTRODUCTION

About five years ago I started developing an Event Timer or chronograph, using the dual frequency vernier system. Described two years ago at the Herstmonceux conference, the Event Timer is near completion and I hope to have at least two Timers built by the end of this year. One of the Event Timers will go to the Yunnan Observatory of the Peoples Republic of China when Mr. Wang Ben-Chun returns to China. Others will be used by Dr. Alley for time synchronization experiments and satellite and lunar ranging.

This paper is organized into three parts. The first part is a description of the fundamental concepts and the equations of the Event Timer. The second part describes the specifications and describes how the Event Timer has evolved since the Herstmonceux conference. The third part concerns the measurement of jitter and a new circuit which improves the jitter characteristics. Final concluding remarks describe a possible new next Event Timer.

Part 1   Fundamental Concepts of the Event Timer

Figure 1 shows the essence of the dual frequency Event Timer concept. One of the dual frequencies, F_1, is produced by a 200 MHz tunable crystal oscillator which is synchronized to a 5 or 10 MHz standard. The 200 MHz oscillator runs continuously to drive a 26 bit synchronous counter which is the time generator. The time generator has exactly 50,000,000 states so it repeats every $\frac{1}{4}$ second.

The second of the dual frequencies, F_2, is produced by a delay line oscillator which is tuned by other circuits to operate at 199.2217899 MHz called 199* MHz. F_1 and F_2 come into synchronization every 257 cycles of F_1 and 256 cycles of F_2. F_2 is derived from F_1 by the equation $F_1 - F_2 = F_2/256$.

An event, either from the test circuit or an outside source, stops, then restarts the 199* MHz restartable oscillator to drive a 9 bit counter called the A register. Constantly monitoring the two frequencies is a comparator which reacts to the rising edges of F_2 and transitions in state of F_1. The result of this operation is that the comparator reacts to the nearest co-incidence of the rising edges of F_1 and F_2. When the F_1 and F_2 rising edges are in closest synchronization, the comparator gives a Sync. pulse which latches or stores the state of the 26 bit time generator and stops the 9 bit A counter.

From the contents of the A and B registers, the epoch of the event can be computed within a 1/4 second interval. The epoch of the event is = Time of Sync. (represented by the number latched in the B register) - the A register count times 5.01953125 n.s.. (5.01953125 n.s. is the period of 199* MHz.)

The vernier action occurs because the period of F_1 and F_2 differ by 19.53125 p.s.. Using the test circuit, which produces an event synchronized to the 200 MHz standard every 1/4 second, we find that A and B repeat every 1/4 second. In figure 2, if the event is delayed by 19.53125 p.s., the Sync condition occurs one cycle sooner, A and B are both decreased by 1.
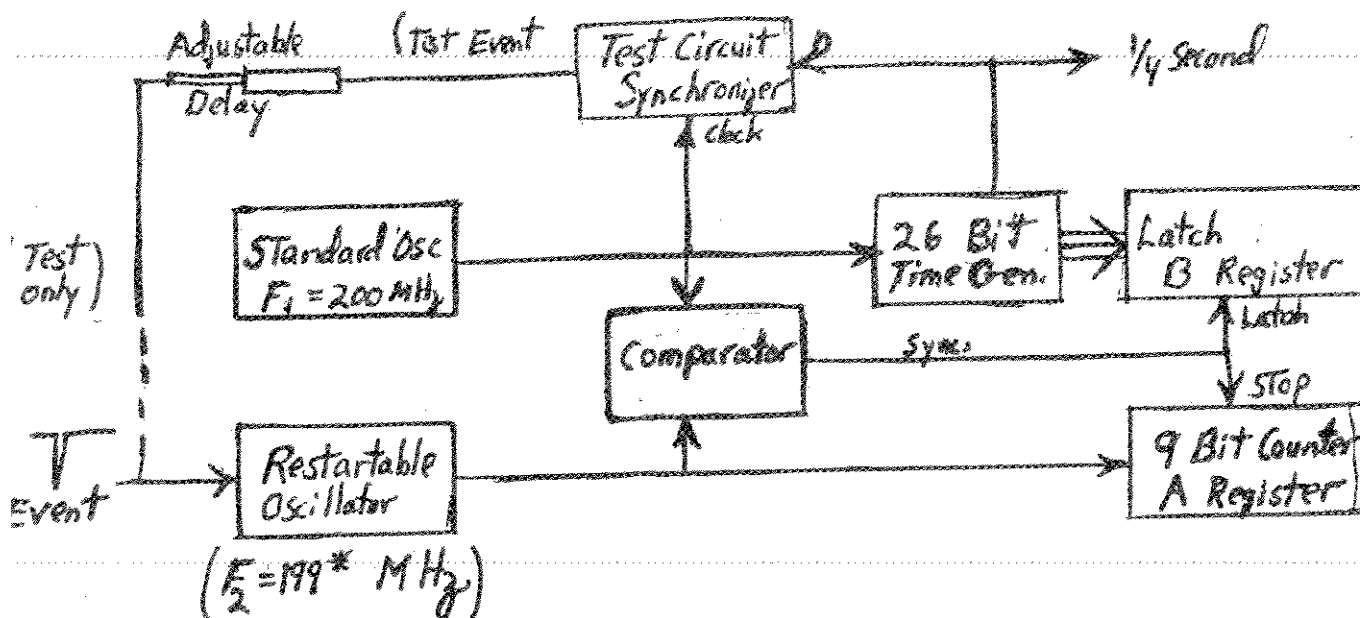
The equation

$$\text{Epoch} = (B-A)(5.0 - A(19.531 \times 10^{-3}) \text{ n.s.}$$

and

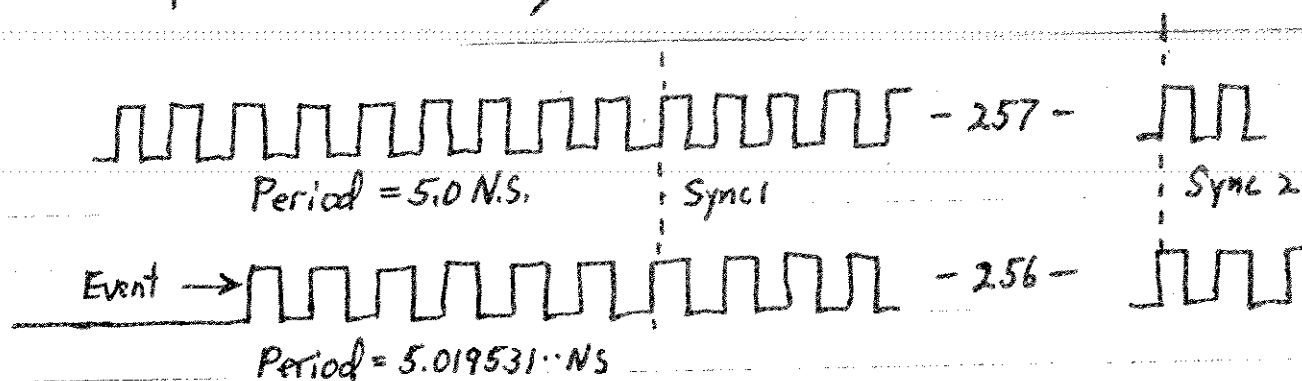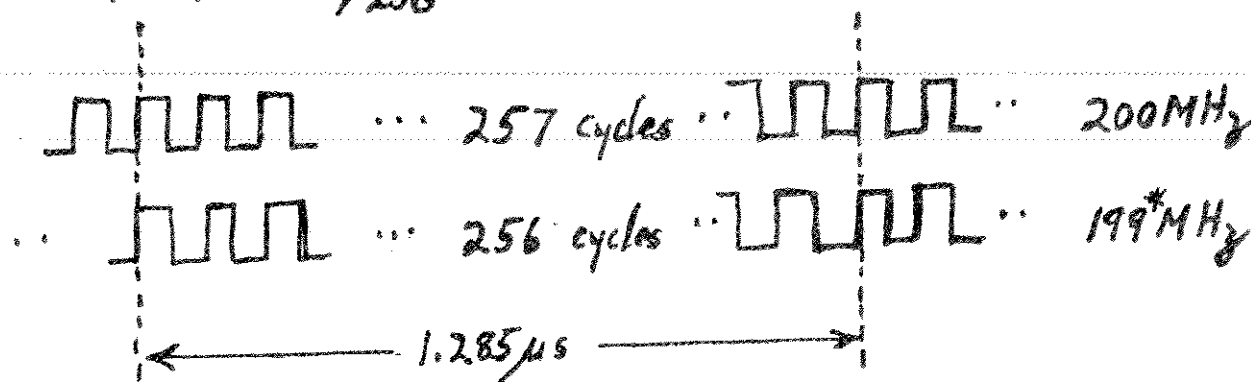$$\text{Epoch}' = \left[(B-1)-(A-1)\right]5.0 - (A-1)(19.531 \text{ E}^{-3}) \text{ n.s.}$$

give

$$\text{Epoch}' = \text{Epoch} + 19.53125 \text{ p.s.}$$

Fundamental Concepts of the Event Timer

figure 1

Adjustable Delay

(Test Event

Test Circuit Synchronizer

¼ Second

Test only)

Standard Osc $F_1 = 200 \, MHz$

26 Bit Time Gen.

Latch B Register

Comparator

Sync

Latch

STOP

Event

Restartable Oscillator

9 Bit Counter A Register

$(F_2 = 199^* \, MHz)$

$$F_1 - F_2 = F_2/256 \qquad \therefore \qquad F_2 = 199.2217899 \, MHz$$

257 cycles · · · 200 MHz

256 cycles · · · $199^* \, MHz$

$1.285 \, \mu s$

$-257-$

Period $= 5.0 \, N.S.$ Sync 1 Sync 2

Event $\rightarrow$ $-256-$

Period $= 5.019531 \cdots NS$

Epoch = Time at Synchronization $- A \, (\, 5.01953125 \,) \, N.S$

Epoch = $B(5.0) - A(5.01953125) \quad N.S.$

Epoch = $(B-A)5.0 - A(19.531 \times 10^{-3}) \quad N.S.$

200 MHz
5.0 NS pe

Sync

Event ⟶

Event Delayed
by 19.531 ps.

New Sync occurrs
1 cycle Sooner
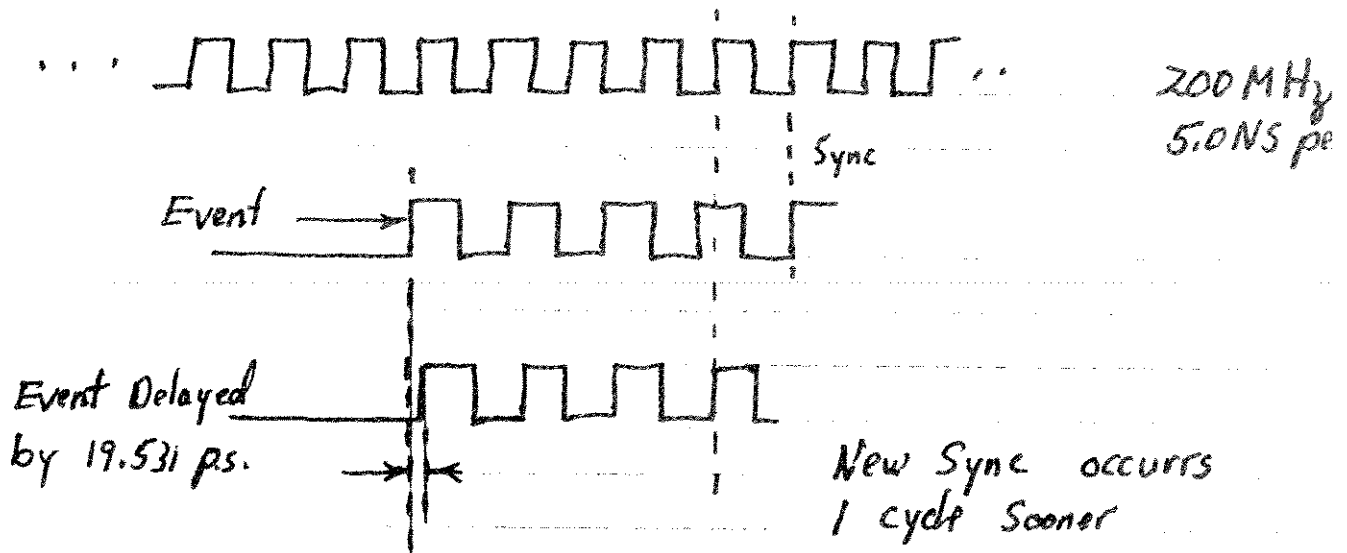
A and B each decreased
by 1 Count

$$Epoch' = \left[(B-1)-(A-1)\right] 5.0 - (A-1)(19.531 \times 10^{-3}) \quad N.S$$

$$Epoch' = (B-A) 5.0 - A(19.531 \times 10^{-3}) + 19.531 \times 10^{-3} \quad N.S.$$

$$Epoch' = Epoch + 19.531 \times 10^{-3} \quad N.S.$$

In General

$$Epoch = \left[(B+257N)-(A+256N)\right] 5.0 - (A+256N)(19.531 \times 10^{-3})$$

$$Epoch = (B-A)(5.0) - A(19.531 \times 10^{-3}) + \left[5.0 - 256(19.53125 \times 10^{-3})\right] N$$

$$\underset{D}{\overset{=}{}}$$

$$Epoch = (B-A)(5.0) - A(19.531 \times 10^{-3})$$

If we can continue increasing the delay of the test event, the Sync. point will come closer and closer to the event. The actual Event Timer is built such that when A becomes equal to about 15, the first Sync. is ignored whereby the next Sync. point 1.285 u.s. later is used. At this time, the A register jumps 256 counts and the B register jumps 257 counts. In fact, any Sync point can be used to compute epoch. In fact, for the Nth synchronization point

$$Epoch = \left[(B + 257N) - (A + 256N) \right] 5.0 - (A + 256N)(19.531 \times 10^{-3})$$

$$Epoch = (B-A)5.0 - A(19.531 \times 10^{-3}) + N(5.0 - 256(19.531 \times 10^{-3}))$$

but $$5.0 - 256(19.531 \times 10^{-3}) = 0$$

$$Epoch = (B - A)5.0 - A(19.531 \times 10^{-3}) \quad n.s.$$

Thus the epoch of the test pulse may be moved about in the 1/4 second interval. Either the first of second Sync. point is used to generate A and B from which the epoch can be computed.

Part 2   Block Diagram and Specifications

        Figure 2 shows a partial block diagram of the Event
Timer. This diagram is useful primarily to show input and
output functions.

        The Event Timer has been expanded to have two independent
verniers. It is thus possible to measure the epoch of two
events up to and including co-incidence. Each event can
arrive on its own cable, or, the events may be combined to
feed both verniers in which case the first vernier arms the
second.

        There are three inputs, each terminated in 50 ohms.
In one mode, input 1 drives vernier 1 only, and input 2
drives vernier 2 only. In the second mode, input 3 drives
both verniers. The input networks accept negative NIM
type pulses going from an initial value of 0 volts to an
amplitude of -.5 to -1.0 volts. Verniers respond to leading
edges, so the pulses may be any width greater than 1 n.s..

        The 200 MHz standard is a 66.66••• Mhz voltage controlled
crystal oscillator with a times 3 multiplier and a very narrow
band filter. The oscillator is phase locked to either 5 or
10 Mhz standards, or, the oscillator may be operated without
a standard at a frequency very close to 200 Mhz..

        The time generator consists of a 24 bit synchronous
counter and two ÷ 2 prescalers adjusted so that the rising
edges of all bits are synchronous. A 27th bit carry is
provided to prevent ambiguity problems if events occur near
the 1/4 second point. The 26 bits and 27th bit carry are
supplied to latches 1 and 2. The 24 bit synchronous counter
number is compared with a 24 bit number supplied by the
microprocessor to form a range gate to enable the Event
Timer. The output of the comparator is filtered by a
glitch supressor to form both a reset pulse for the A
registers and a rising edge to enable the input gate portions
of the phase disconnect circuits. The microprocessor
supplies an inhibit pulse to the glitch supressor to prevent
false range gate pulses while the numbers are being updated
in the comparator. The range gate may be opened on the
next 20 n.s. clock pulse following an external NIM type pulse.

Partial Block Diagram of Event Timer — figure 3
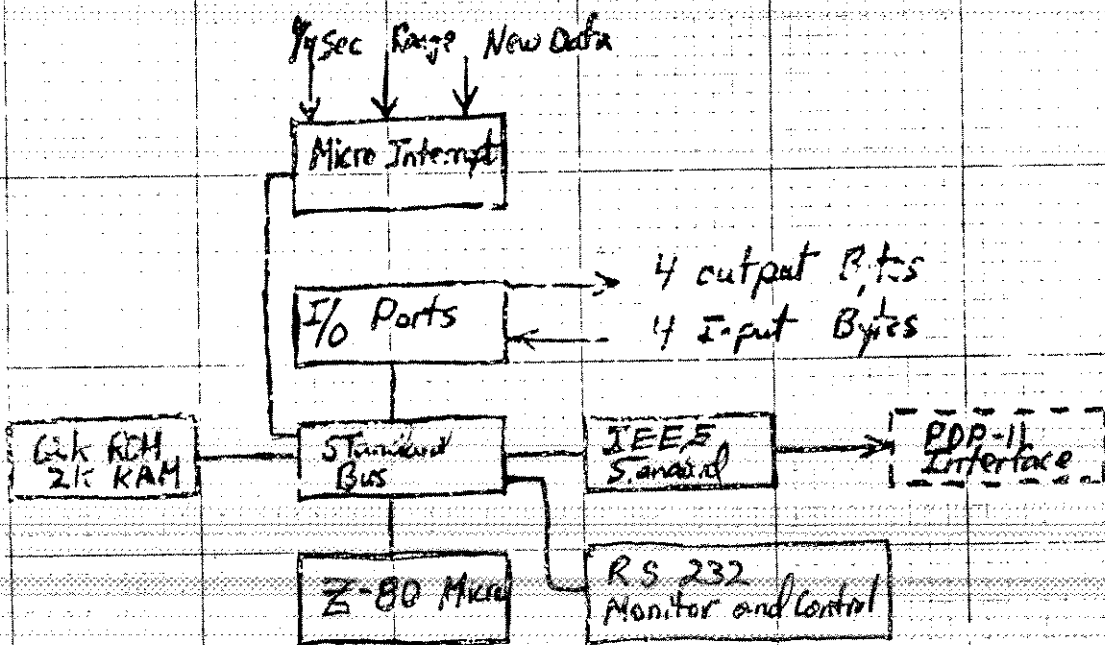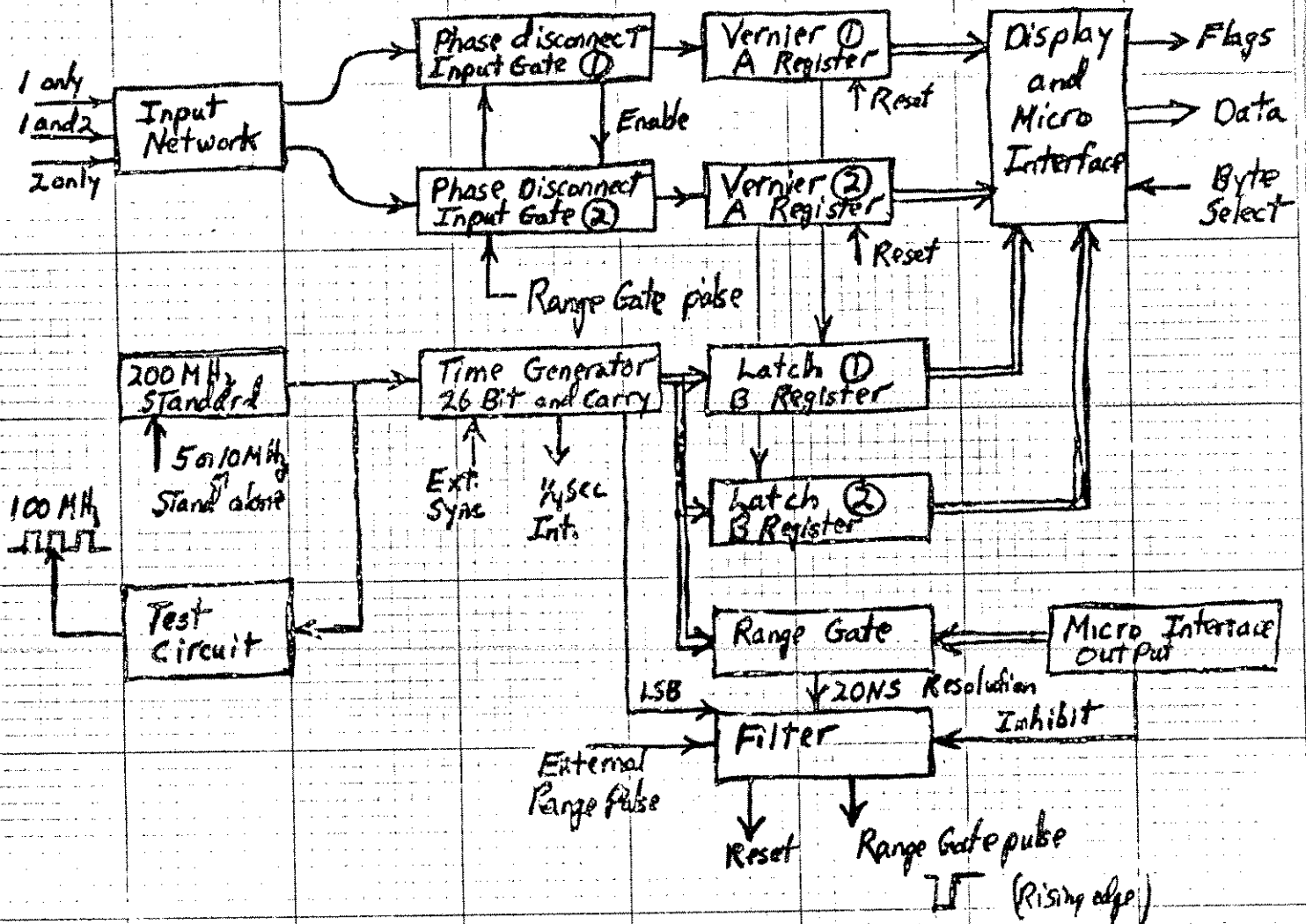
The phase disconnect circuit ① is enabled by the trailing edge of the range gate pulse. Phase disconnect circuit ② is enabled by either the same range gate pulse if the verniers are to be enabled simultaneously, or, phase disconnect circuit ② may be enabled when circuit ① has received an event to allow operation in the serial mode.

The outputs from the A and B registers are displayed with LED readouts and are stored in two 40 bit storage registers. The Z-80 microprocessor receives program interrupts when new data is available, when the range gate goes off, and when the 1/4 second pulses are generated from the time generator. The microprocessor reads in the data one byte at a time and can tell how much data is available by reading data status flags. Because the A and B registers act as storage registers along with the two 40 bit storage registers of the interface, it is possible to store four epochs, two from each vernier before the data must be read out. This feature provides for very rapid acquisition of data for very close targets.

The micro computer has 62K of ROM and 2K of RAM. The system operates the IEEE bus and RS-232 type monitors. Programs have been developed in FORTH language to calculate epoch and time of day and various tests for the Event Timer.

The Event Timer in conjunction with the Z-80 can give range data to the mainframe system computer at a rate of 172 ranges per second or every 5.8 milliseconds. However, the Event Timer can operate by itself every 7 microseconds or at a rate exceeding 100,000 ranges per second for each vernier.

Through the kindness of Messieurs Dachel and Ingold of the Bendix Corporation, the Allen Variance and the harmonic content of the 200 MHz standard were measured. Jeff Ingold's report is shown in figure 4.

CHARLES A. STEGGERDA

figure 4

9-4-86

200 MHz PHASE LOCKED OSCILLATOR

VECTRON S/N 628441   PHASE LOCKED TO NP 2 vs NP 4

TAU	ALLAN VARIANCE (σ_y^2)		FLOOR
0.1 second	1.00 E -11	500 samples	6.49 E -12
1.0	2.39 E -12	500	8.43 E -13
10	2.08 E -13	100	1.00 E -13
100	3.30 E -14	5	1.53 E -14

HARMONICS

2ND (400 MHz)   > 56 dB down from CARRIER

3rd (600 MHz)   > 60 dB down from CARRIER

4th (800 MHz)   > 60 dB down from CARRIER

SUB HARMONICS & SPURIOUS RESPONSE
> 70 db down from CARRIER

ALLIED Bendix
Aerospace

9-4-86

JEFF INGOLD

964-7188

Part 3   Jitter Measurements and a New Phase Disconnect Circuit

Consider again the basic block diagram of figure 1. If an event is generated precisely every 1/4 second and this event is synchronized to the 200 MHz standard, then the A counter and B latch will repeat the same numbers every 1/4 second. This in fact does happen, the same epoch being calculated for 10 to 20 minutes at a time with no jitter.

This test mode is not however the way the Event Timer is to be used. In operation the range gate operates 10 to 100 times a second in varying patterns according to the laser firing and the expected return time. A more valid test would replace the 1/4 second period pulse with a pulse from an ordinary free running pulse generator running at 30 pps.. In this mode an event is generated that is synchronized to the 200 MHz standard but comes at a random time in the 1/4 second interval. In this mode the A counter value should be constant and the B latch value should constantly change. The Event Timer of 6 months ago however had a jitter of up to 8 counts on the A counter when the range gate was moved randomly yet the A count was very stable if the range gate was opened at precise intervals as generated by the time generator. Measurement of the interpolator assembly of the Hewlett Packard 5370 universal counter revealed the same problem, which is understandable since the Event Timer verniers are directly related to H.P. interpolators.

It appears that an improvement can be made in the system jitter if F_2, the 199* MHz oscillator, is stopped and restarted in a controlled manner. In the original fixed delay phase disconnect circuit, a 10 n.s. pulse synchronized to the event to be measured, stops and restarts F_2. Before this synchronization process, the event is in no way synchronized to F_2, and so the oscillator is stopped at any point in its cycle as shown in figure 5. When the oscillator is restarted, the initial conditions vary depending on what part of the cycle the oscillator was stopped. The changing initial conditions cause a phase jitter in F_2 relative to the event which then is measured as a system jitter.

The Action of Phase Disconnect Circuits   Figure 5

A. Fixed Delay Phase Disconnect F_2 Waveforms (Pin 11)

Individual
Snapshots
Synchronized To Event

Multiple
Exposures

|← Fixed Delay →|
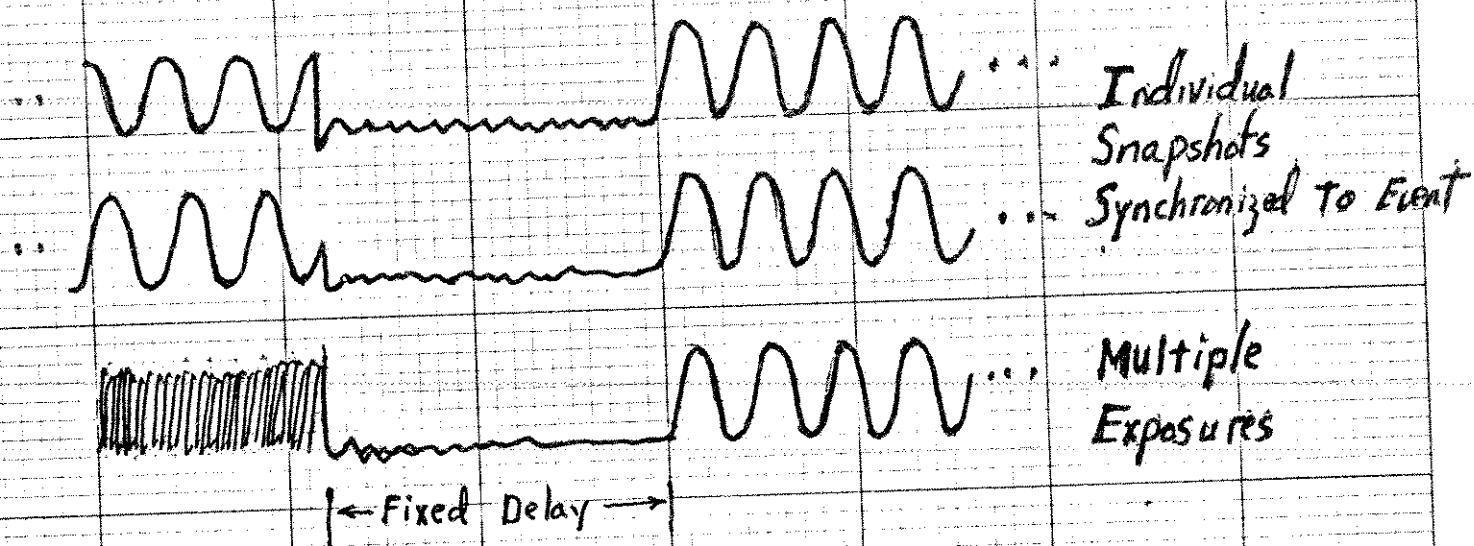
B. Variable Delay Phase Disconnect F_2 Waveforms

A different way to stop F_1 would be to allow the oscillator to complete its current cycle and always stop at the same minimum voltage. Then, after the transcients have subsided, restart the oscillator synchronized to the event. This variable delay phase disconnect technique has the same conditions at turnoff but a variable delay time for the transcients to subside. The fixed delay phase disconnect technique has differing energies stored in the oscillator at turn off but a fixed delay time for the transcients to subside. The variable delay seems to result in less phase noise. Further improvements can be made by increasing the delay before restart.

Jitter measurement have been made on five H.P. restartable oscillators in the Event Timer. The test event was a 100 MHz square wave synchronized to the 200 MHz standard. The range gate was opened randomly on the next 20 n.s. window by a free running pulser running at about 30 p.p.s.. The range gate opening is synchronized by the 50MHz least significant bit of the time generator to prevent slicing of the event pulse. 100 sample runs were made for all values of the vernier and the RMS jitter was calculated. The results are shown in figures 6,7, and 8.

Use of this variable delay phase disconnect circuit has resulted in a reduction of jitter from perhaps 35 p.s. RMS to the order of 15 p.s. RMS at this time. Further improvements may be possible. While this reduction may not be important in Lageos tracking where there is an abundance of data to smooth out the jitter, this should be a decided advantage in Lunar ranging where every data point is precious.
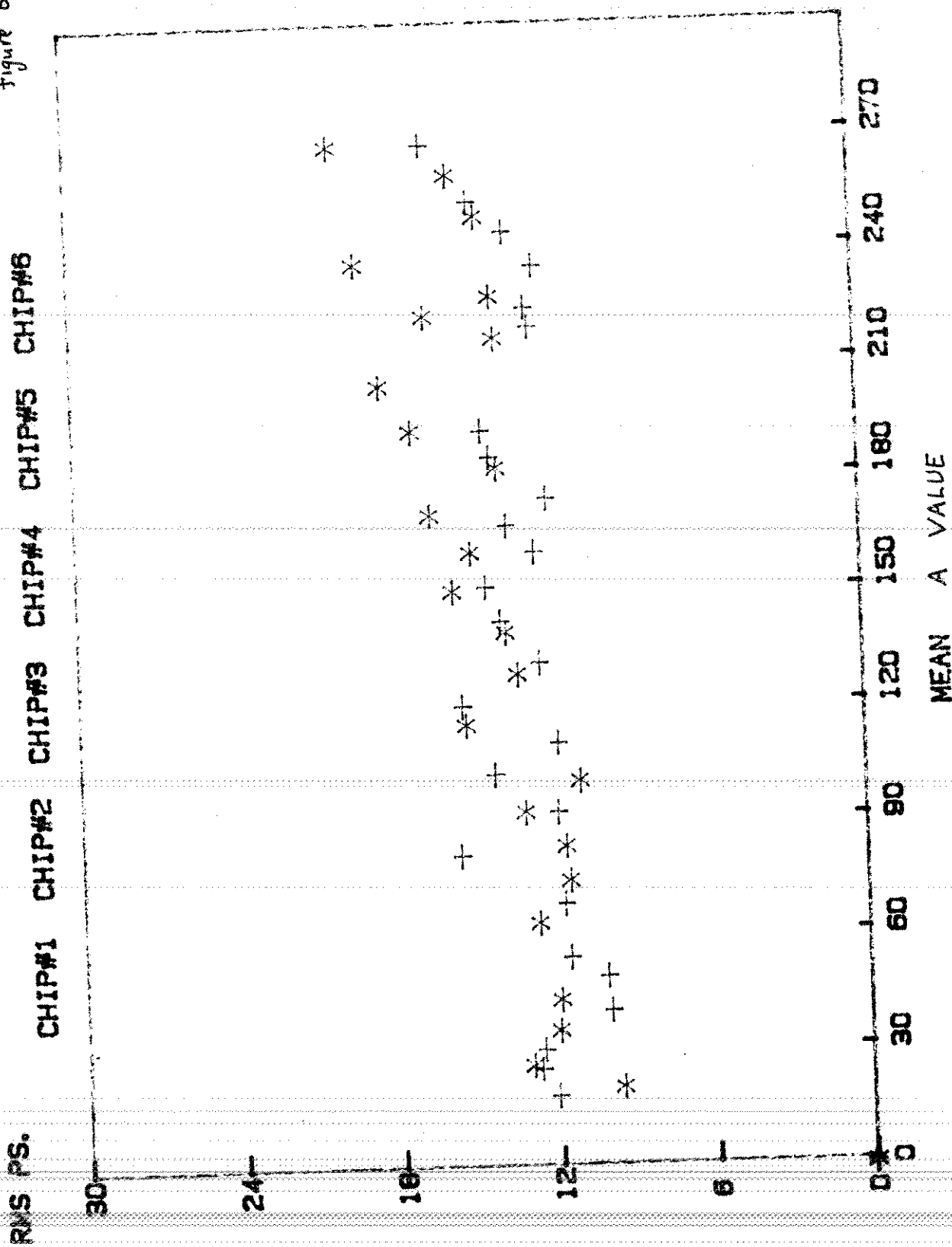
Again, using the above described test of measuring a 100 MHz square wave at random times, a test was made over a period of one hour of the stability of the system. During the test, the delay line was not changed, the temperature was held constant at 22.5 C., and 1000 measurements were made and averaged every two minutes. The mean value of each 1000 measurements is plotted in figure 9.

Further tests, which have not been done as yet, would measure the linearity of the vernier. In this linearity test, the standard used to generate the test signal would be allowed to slowly drift with respect to the standard of the Event Timer. If measurements were made at precisely known times, the rate of drift could be measured and a projected ideal vernier could be formulated. The deviation from this ideal vernier would measure the linearity error.
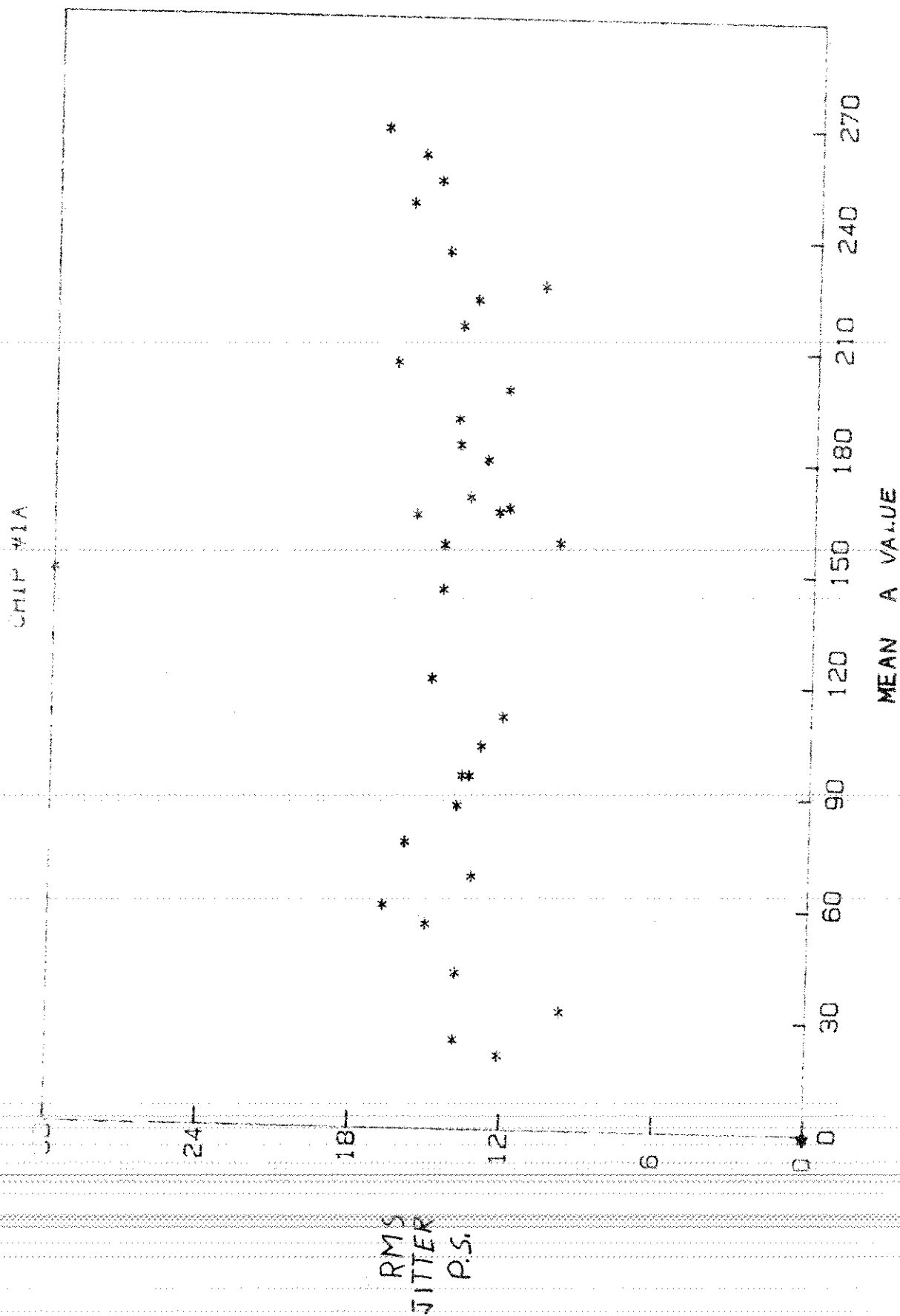
EVENT TIMER RMS JITTER

CHIP#1 CHIP#2 CHIP#3 CHIP#4 CHIP#5 CHIP#6

+ — Chip 2
* — Chip 5

figure 6

RMS PS.

MEAN A VALUE

EVENT TIMER RMS JITTER

CHIP #1A
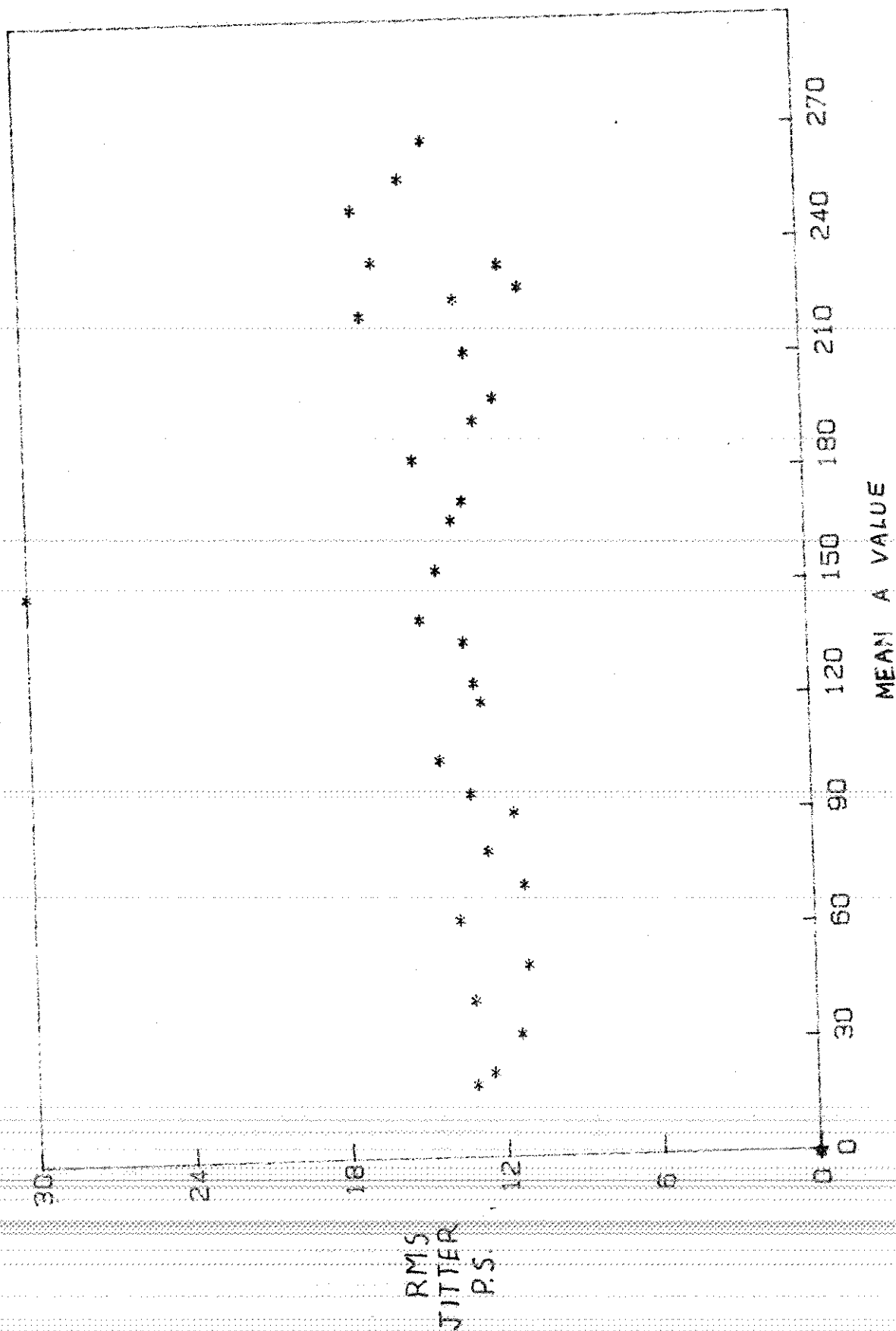
RMS
JITTER
P.S.

MEAN A VALUE

figure 7

EVENT TIMER RMS JITTER

Figure 8

P.S. Mean Value of 1000 Measurements of 100 MHz Clock Measured at Random

150 microns

P.S.
619
618
617
616
615
614

11:05 A.M. 11:15 11:25 11:35 11:45 11:55 12:05 P.M.

TIME   Nov. 5, 1986

figure 9

Finally, I have been asked whether a 10 p.s. resolution Event Timer could be made using the H.P. restartable oscillator. It is not practical to use the H.P. chip in its present form because the transmission line oscillator cannot be stabily tuned to the required 199.610136.. MHz. In this mode of operation there would be 513 of the 200 MHz. cycles for 512 of the offset frequency giving a resolution of 9.76 p.s.

If, as is shown in figure 10, an entirely new restartable oscillator were to be made, I believe that it is possible to design an Event Timer based of the standard frequency of 400 MHz. Using 512 as the offset frequency divider instead of 256, the restartable oscillator frequency becomes 399.2202729 MHz with a period of 2504.882813 p.s.. The resolution of the Event Timer is 4.88 picoseconds. Hopefully, the RMS jitter could be less than 5 p.s..

Design of 400 MHz Event Timer

Figure 10

1) $F_1 = 400 \, MHz$

2) Time generator is a 27 Bit, Synchronous Counter consisting of 3 $\div 2$ prescalers and the present 24 Bit counter.
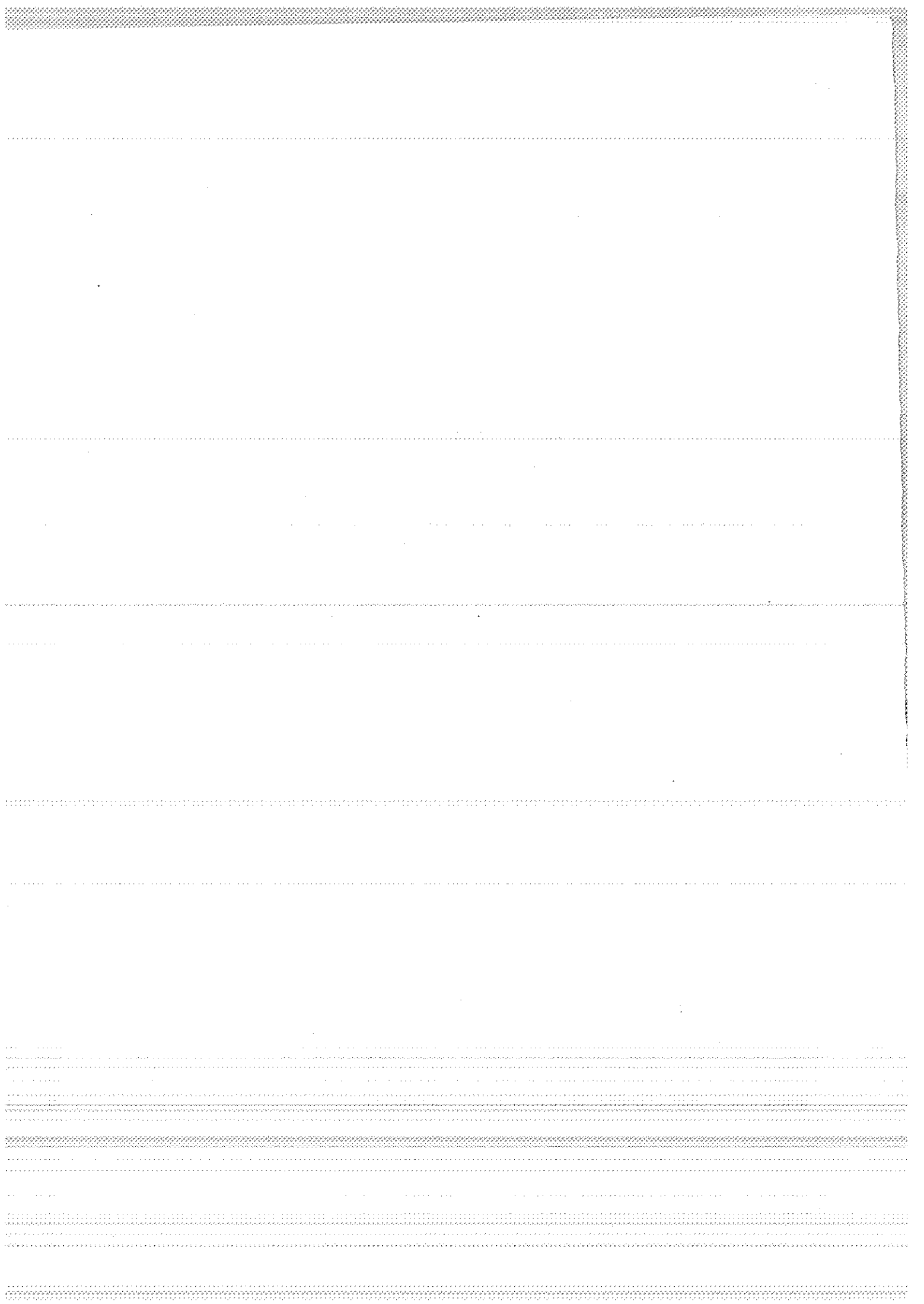
3) Resolution of Range Gate   20 N.S.

$$F_1 - F_2 = F_2/512 \qquad\qquad F_2 = 399.2202729 \, MHz$$

$$\frac{400 \, MHz}{513} = .77972 \cdots MHz \quad \text{Beat Frequency}$$

$$2500 \left(\frac{513}{512} \right) = 2504.882813 \cdots = \text{period of } F_2 \quad P.S.$$

Period of $F_1 = 2500 \, P.S.$

4) Resolution of Vernier $= 4.8828 \, p.s.$

STABLE SATURABLE DYE FOR 1.06 μM

K. Hamal, H. Jelinkova
Czech Technical University
Faculty of Nuclear Science and Physical Eng.
Brehova 7, 115 19 Prague 1 - Czechoslovakia -

Telephone 848840
TWX 121254 FJFI C

ABSTRACT

Most of the second generation Satellite and Lunar ranging stations and practically all of the 3. generation ones exploit pico-second pulses to ensure the required accuracy. To synchronize the modes and to Qswitch the resonator, either an active or passive modulator or combination of them, may be used. To apply a passive modelocker/Qswitch, some characteristics of the saturable modulator (bleacher) are required.

STABLE SATURABLE DYE FOR 1.06 μm

Karel Hamal, Helena Jelinkova

Most of the second generation Satellite and Lunar ranging stations and practically all of the 3.generation ones exploit picosecond pulses to ensure the required accuracy.To synchronize the modes and to Qswitch the resonator,either an active or passive modulator or combination of them,may be used.To apply a passive modelocker/Qswitch,some characteristics of the saturable modulator (bleacher) are required:

- compatability with the Nd transition and host (YAG,YAP, Nd glass,etc) (wavelength, absorption cross-section, lifetime,saturation intensity)
- short/long term stability
- acceptable solvent
- to range Satellites/Moon,the desirable pulse duration is 30-100 psec (3.generation) and 30 psec or less for 4.generation /1/.

We have worked to develop saturable dye having performances closed the mentionned ones above.The parameters of the resulting saturable dye ML51 /2/ are summarized in the table 1.Some other dyes are mentioned for comparison.

The photostability has been estimated from the following experiment: the sample of the dye was illuminated by the cw high pressure xenon flash lamp XBO500 /3/. The exposure time of the photodecomposition was measured and the slope was compared for different dyes (Fig.1.).

To investigate modelock/Qswitch properties, we have used different laser configuration:
(1) /4/ The YAG rod was cut at 1 deg near the back mirror, the perpendicular surface on the opposite side acted as the output mirror. A 5 mm cell, containning 2 cc of no flowing dye, was placed at the Brewster angle between the back mirror and the YAG crystal. The optical length of the resonator was 30 cm. The single mode operation was accomplished by an iris 1 mm in diameter. The output energy was 3 mJ in a train of two or three pulses, the reprate was 2.5 Hz. The pulse duration and the output energy fluctuation were detected and statistically processed using a diagnostics chain consisting of the second harmonic generator, the streak camera Hamamatsu C-979 (10 psec resolution) interfaced with the SIT camera and temporal analyzer, the HP85 console and

the computer HP 1000. The resulted pulse duration at 0.53 um was 30 psec RMS, the output energy 3mJ, RMS = 3% (Fig.2A). The corresponding power density is 3 GW/cm^2. To examine the output spatial structure of the beam, the detection chain /5/, consisting of the CCD Fairchild camera, Quantex singleframe memory and HP 1000 has been used. The beam profile is closed to the Gaussian. (Fig.3.) The divergence is 1 mrad, close to the diffraction limit. The corresponding brightness is 3.10^{15} W/cm^2 sr.

(2) To prove the saturable dye in the active/passive arrangement, we put it to Quantel laser system at CERGA (fall 1983). The oscillator contains a dye cell and a active modelocker. The records of the output pulse train and selected pulses are on Fig.4. The transmission of the bleacher has been set to obtain required 5-7 pulses within FWHM envelope. The reprate was 10 Hz. A similar experiment was carried out at U. of Maryland /10/ using Kodak 9740 and ML51. Pulse widths were between 20-50 psec, however the shot to shot energy stability of the cavity dumped single pulse was poor.

(3) The ML51 was applied in two wavelength experiment /6/. To obtain picosecond ranging accuracy, the pulse duration should be minimized. The oscillator consisted of the concave 5m, 100%, back mirror in contact with 2 mm flowing dye cell. The YAG rod 3 mm in diameter 2deg/2deg AR coated was pumped in Quantel head. The front mirror was a quartz plate 0.25 mm thick. The duration was 14 psec at 0.53 um, when deconvoluted. The pumping energy was varying up to 2.3 times above the modelock threshold and no change in the pulse duration or stability has been observed.

(4) The saturable dye was used to modelock the YAP laser /7/. The laser setup was similar to the experiment in (1). The raw value of the pulse duration was 10 psec, actually equal to the temporal resolution of the streak camera.

Generally, we did not observed any damage of any optical element throughout all experiments and during long term exploitations in different laser configurations. The saturable dye ML51 has been used at the INTERKOSMOS satellite laser station in Egypt since 1982 /1/, for two wavelength experiment /9/, for the ophtalmology and in several other lasers, occationally, the dye lasts in the cell for several months.
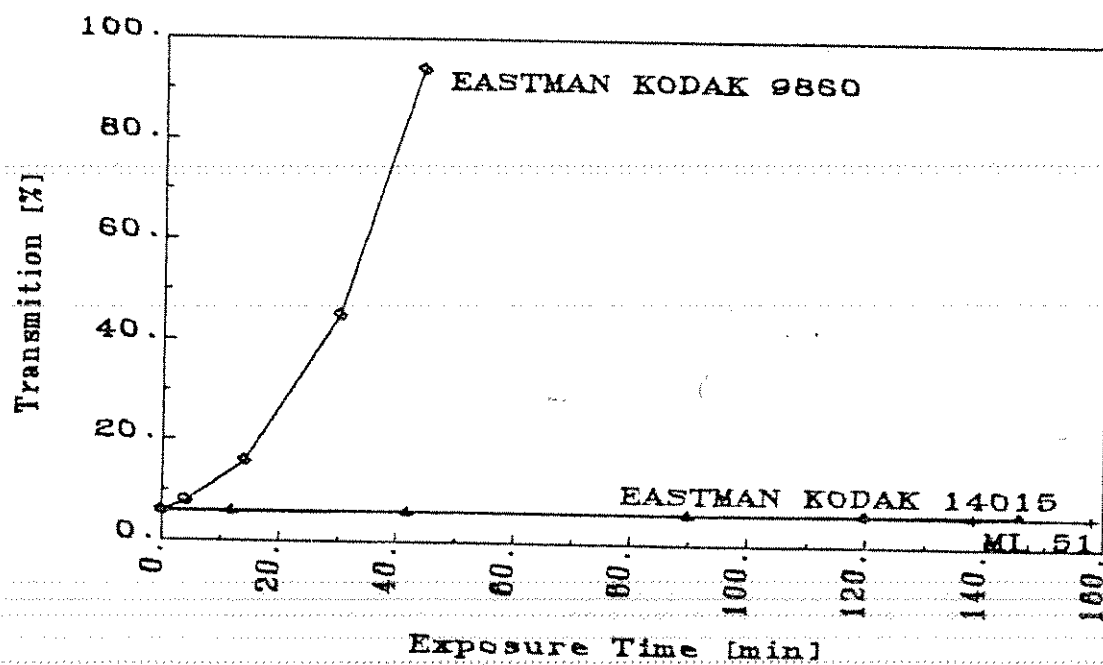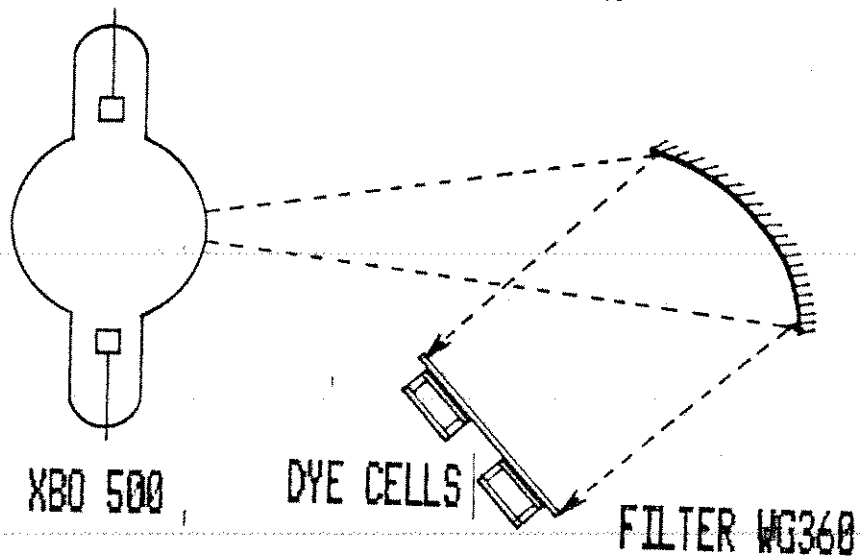
LITERATURE

/1/ Proceedings of the V.International Workshop
    on the Laser Ranging Instrumentation,Greenwich,1984.
/2/ K.Hamal,H.Jelinkova,V.Hruskova,CLEO,Baltimore,May,1985
/3/ B.Kopainski et al, Appl.Phys., 15,1982,p.29.
/4/ H.Jelinkova, in /1/
/5/ H.Jelinkova, in this Proceedings.
/6/ J.Gaignebet et al, in this Proceedings.
/7/ K.Hamal, to be published.
/8/ K.Hamal et al, in /1/.
/9/ V.A.Babenko et al, Quantum Electronics,
    7, 1980, p.1796, (in Russian).
/10/ W.Koechner, Solid-State Laser Engineering, Springer-
    NY, 1986
/11/ I.Prochazka, in this Proceedings.
/12/ M.Košelja, MS thesis.

Parameters of saturable dyes				
	ML51 /2/	3955	Kodak 9740	Kodak 9860
Solvent	dichloethane	etylalcohol	chlorbenzen	dichlorethane
Molec. weight	631	600	762	
λ_{MAX} (nm)	1010	1040 /9/	1049	
G_{MAX} $(10^{-16} cm^2)$	5.54		6.2	
G_{1060} $(10^{-16} cm^2)$	0.45	3.2 /9/	5.7	3.5
τ (ps)	37+/-2	40 /9/	8.3 /10/	9.3 /10/
I_s (MW/cm^2)	.112	7.3 /9/	40 /10/	56 /10/

Tab.1.

PHOTOSTABILITY TEST

EXPERIMENTAL ARRANGEMENT

XBO 500   DYE CELLS   FILTER WG360

EASTMAN KODAK 9860

EASTMAN KODAK 14015

ML 51

Transmition [%]

Exposure Time [min]

K.Hamal, H.Jelinkova
Stable Saturable Dye For 1.06μm

1

LASER OUTPUT

MLT

500 psec/div
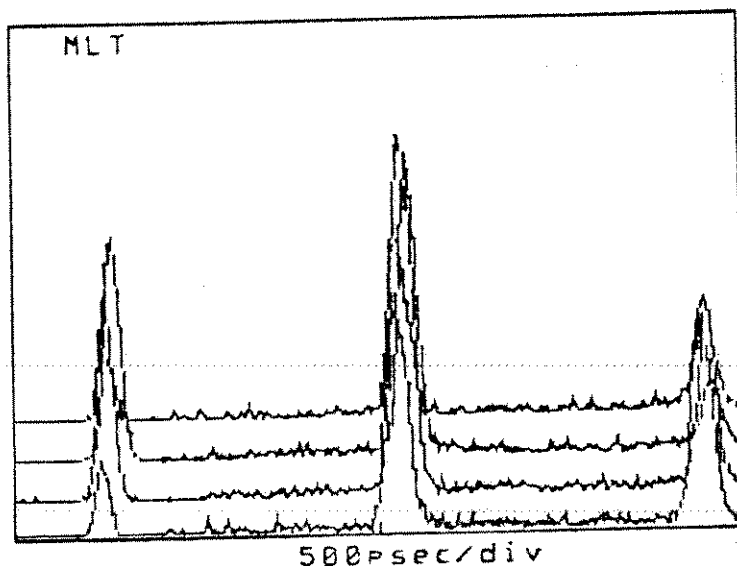
MODELOCKED TRAIN

(STREAK)
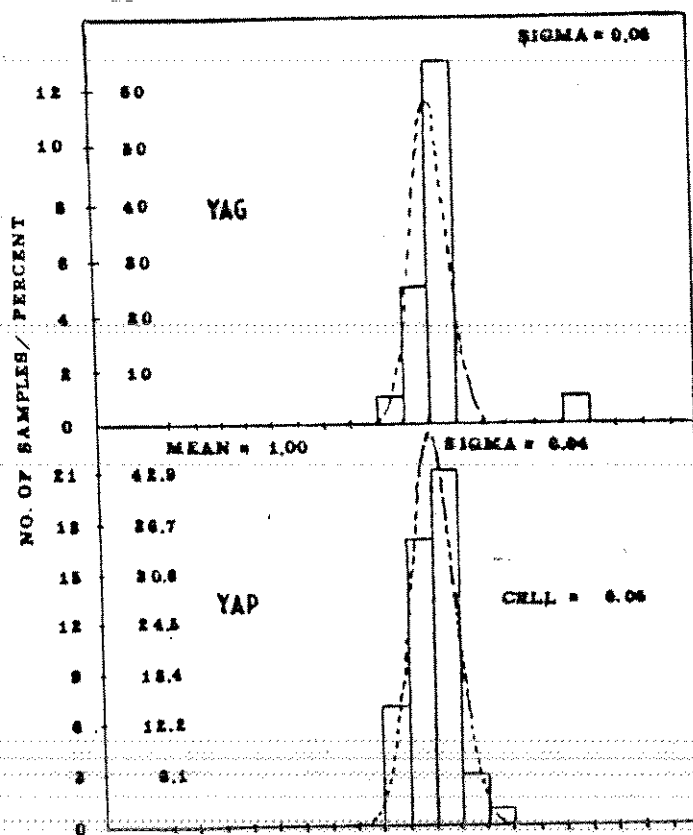
ENERGY STABILITY

HISTOGRAM

SIGMA = 0.06

YAG

MEAN = 1.00   SIGMA = 0.04

YAP   CELL = 0.05

K.Hamal, H.Jelinkova
Stable Saturable Dye For 1.06 μm

2

SPATIAL STRUCTURE OF THE OUTPUT BEAM

OSCILLATOR BEAM
DIVERGENCE 1 MRAD
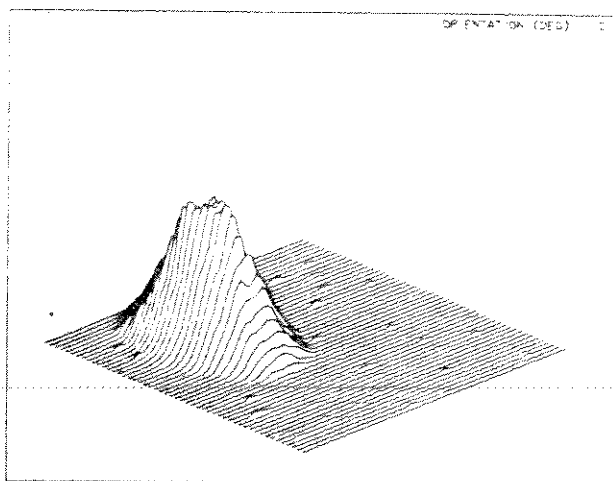
GAUSS PROFILE
(THEORY)

DIFFERENCE ~ 8%

K.Hamal, H.Jelinkova

Stable Saturable Dye For 1.06μm

3

INTERKOSMOS SATELITE LASER RADAR NETWORK

ACTIVE/PASSIVE MODE LOCKED LASER OUTPUT TRAIN

K.Hamal, H.Jelinkova

Stable Saturable Dye For 1.06μm

4

SPATIAL STRUCTURE OF THE DOUBLED Nd : YAG LASER TRANSMITTER BEAM

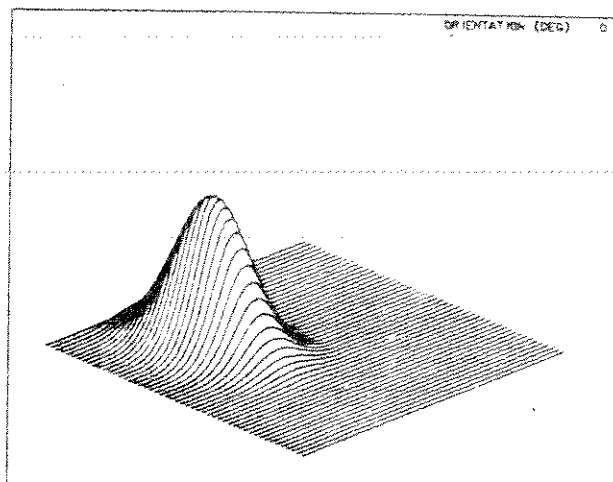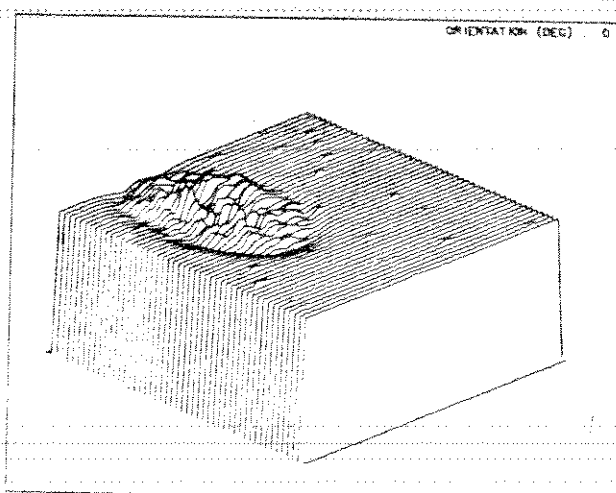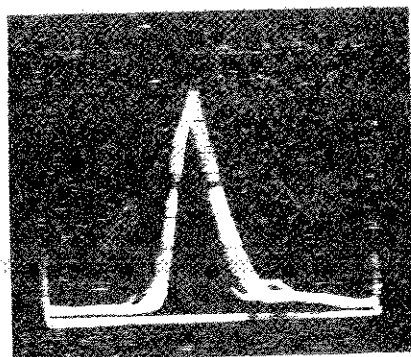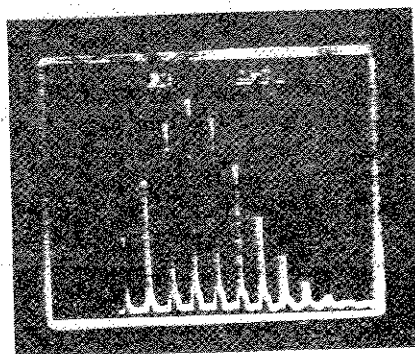H. Jelinkova, P. Valach
Czech Technical University
Faculty of Nuclear Science and Physical Eng.
Brehova 7, 11519 Prague 1 - Czechoslovakia -

Telephone 848840
TWX 121254 FJFI C

J. Del Pino
Cuban Academy of Sciences
Institute for Geophysics and Astronomy
Santiago de Cuba

ABSTRACT

The beam spatial structure of the passively mode-locked Nd : YAG oscillator/amplifier/SHG laser radar transmitter has been examined.

To analyze the laser beam structure, an on line diagnostic chain, giving a three-dimensional graphic display, the contours and the two dimensional Fourier transformation of the output pattern was implemented at the Interkosmos indoor calibration facilities.

The beam was studied in every point of the laser transmitter and the IR Gaussian beam structure changes due to the outside oscillator optical elements were eliminated from the system. The SH beam profile was investigated from the point of view of temperature dependent efficiency and the pointing stability. The difference between the spatial shape of pulse IR and SH was found and the changes between them were tried to be compensated by the help of the tandem scheme of two SHG crystals.

SPATIAL STRUCTURE OF THE DOUBLED Nd:YAG LASER TRANSMITTER BEAM

H.Jelinkova, P.Valach, J.del Pino

INTRODUCTION

A Nd:YAG laser (YAG, YAP, etc.) allows to generate picosecond pulses for laser ranging. However, up to now, a lack of detectors in the near IR requires the radiated frequency to be multiplied into the second resp.third harmonics. To apply a second harmonic generator (SHG) into the laser transmitter scheme, the homogeneous, Gaussian IR output beam is required. Every change of the laser system configurations (resonator readjustement, active or passive elements temperature dependence, pumping inhomogeneity, etc.) causes significant changes of the Gaussian beam structure. Applying the new technology giving the fast accurate response, we have got the possibility to optimize the laser system performance. Consequently, the spatial structure of the transmitter output SH beam has been investigated.

EXPERIMENTAL ARRANGEMENT

The laser system configuration /1,2,3/, we employed, consists of passively mode-locked Nd:YAG oscillator, isolation saturable dye cell, expanding telescope, single pass amplifier and KDP doubling crystal (Fig.1.). According to /4/ the image in the focal plane of a well corrected lens coincides with the beam far field pattern (in Fraunhoffer region). Therefore, in the laboratory, the beam farfield was observed in the focus of the 2.5 m thin lens by the help of the CCD array (Fairchild 320 x 489 cells). The CCD output signal was digitized using Quantex image memory (256 x 256 cells, 8 bits, 100 MHz) and stored on line on the magnetic disc of the host computer (Fig.2.).

IR BEAM

To understand the beam distortion through the laser transmitter, the beam was examined at different points (Fig.1,Fig.3) (behind the oscillator (A), the isolation cell (B), the expanding telescope (C), the amplifier (D)). The oscillator output beam structure was clean, near Gaussian, with the divergence of the one mrad (Fig.3A). The greater increment to the distortion was made by the isolation 5 mm thick Brewster angled dye cell (Fig.3B). The improvement was

obtained by tilting the dye cell to 1 degree. Resultant divergences
in every measured points are summarized in Tab.1.

SH BEAM

In general case, the index of refraction of the negative
nonlinear crystal, which is mostly used in SHG, depends on the
incidence angle θ, the temperature T and the basic radiation
wavelength Λ. Every change of these parameters causes the index
matching condition modification.

In our experiment, the temperature dependence of the SHG was
investigated in detail.
1) The temperature of the SH crystal was varied from the 16°C
to 37°C and the index matching angle was found for every examined
temperature. From Fig.4 it can be seen that there is no variation
in the efficiency within the experimental limit and therefore in
the measured temperature interval the optimal thermal region for
dominating SH output does not exist.
2) The index matching angle was alligned for the 24°C and the
temperature dependence of the efficiency and the spatial structure
was investigated. For the KDP crystal type II the temperature
dependence is expressed by /5/:

$$\Delta T = \frac{0.44 \Lambda}{L} \cdot \left(\frac{\partial n_e^{2\omega}}{\partial T} - \frac{\partial n_o^{\omega}}{\partial T} \right)^{-1}$$

where Λ is the wavelength of the incident wave, L is the crystal
length, T is the temperature. For the KDP crystal (10x10x30 mm)
which was used to SH conversion $\Delta T_{CALC} = 5.8°C$. (ΔT is the interval
in which the efficiency is more than 1/2 of maximum value). This
calculated value coincides with the experimental measured data
plotted on Fig.5 from which follows $\Delta T_{EXP} = 6.2°C$. The independent
experimental determination was done by the integration of the CCD
output spatial structure.

From the measuring of the temperature dependence of the far
field SH beam spatial structure (Fig.6) follows that inside the
temperature range 24°C-32°C, the SH beam has mostly clean profile
and due to the diffraction aperture effect, the contour has a
little elliptical form. Within the range 18°C-22°C, the beam
profile was deformed and in the temperature range 36°C-52°C, the
most significant feature observed was the appearance of a double
spot alternating regularly with the homogeneous elliptical one.
In all cases, the center of the beam has been shifted with changing
temperature.

In Fig.6. it is seen that the far field beam structure of the SH beam has the elliptical form. This distortion of the spatial structure in one direction follows from the fact that due to the double refraction of the nonlinear crystals, the extraordinary ray deviates in the anisotropy or walk off angle. The beam of the SH radiation is therefore deviated from the original (IR beam) direction and from this fact the aperture effect follows which decreases the efficiency of the SHG and changes the shape of the pulse (Fig.7.B). We try to use the tandem scheme /7/ for the compensation of this deviation. The resulted spatial beam structure is on Fig.7.C.

SUMMARY

The laser transmitter system was designed to have an optimum farfield beam spatial structure what implies a good farfield and a higher efficiency of the SH radiation beam. The measurement of the temperature dependence of the SH crystal showed the strong dependence of the efficiency, of the spatial structure and of the pointing accuracy on temperature changes.

LITERATURE

/1/ Jelinkova H., Proceedings of the Vth International Workshop on Laser Ranging Instrumentation,Greenwich, England, 1984.

/2/ Hamal K., Hruskova V., Jelinkova H., Proceedings of CLEO 1985, Baltimore, USA.

/3/ Hamal K., Jelinkova H., "Stable Saturable Dye for 1.06 um", in this Proceeding.

/4/ Born M., Volf E., "Principles of Optics", Pergamon Press, 1964.

/5/ Koechner W., "Solid-State Laser Engineering", New York, Springer Verlag, 1976.

/6/ Tarasov L.V., Dmitrijev V.G.,"Prikladnaja Nelinejnaja Optika", Moskva, Radio i Svjaz, 1982 (in Russian).

/7/ Volosov V.D. et al., Sov. J. Quantum Electron., 6, p.1163, 1976.

Tab.1. Laser System Divergence

A) Isolation cell – Brewster angle

Measured point	X [mrad]	Y [mrad]
A	1	0.9
B	1.7	1.1
C	0.8	0.6
D	0.7	0.6

B) Isolation cell – 1 deg angle

Measured point	X [mrad]	Y [mrad]
A	1	0.9
B	1.1	0.9
C	0.6	0.6
D	0.6	0.6
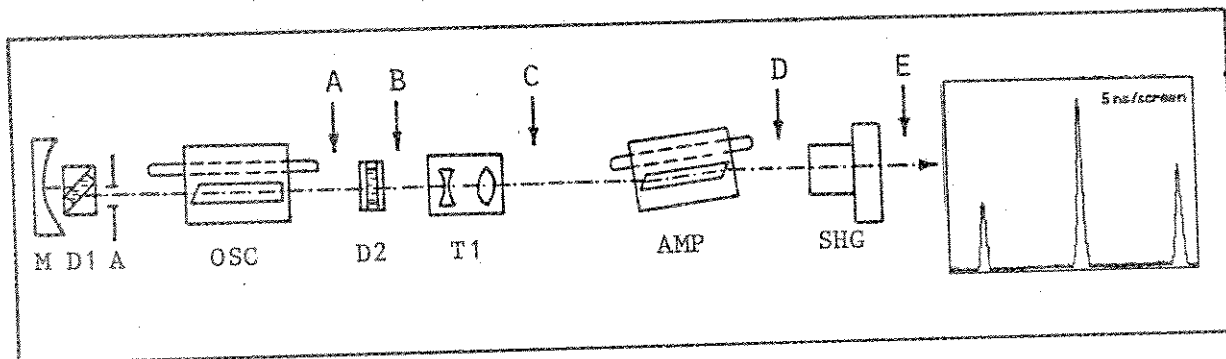
Fig.1. Block diagram of the optical lay-out of the Nd:YAG laser transmitter.

M	End mirror	D2	Dye cell
D1	Dye cell	T1	Telescope
A	Aperture	AMP	Amplifier head
OSC	Oscillator head	SHG	KDP II Frequency doubler
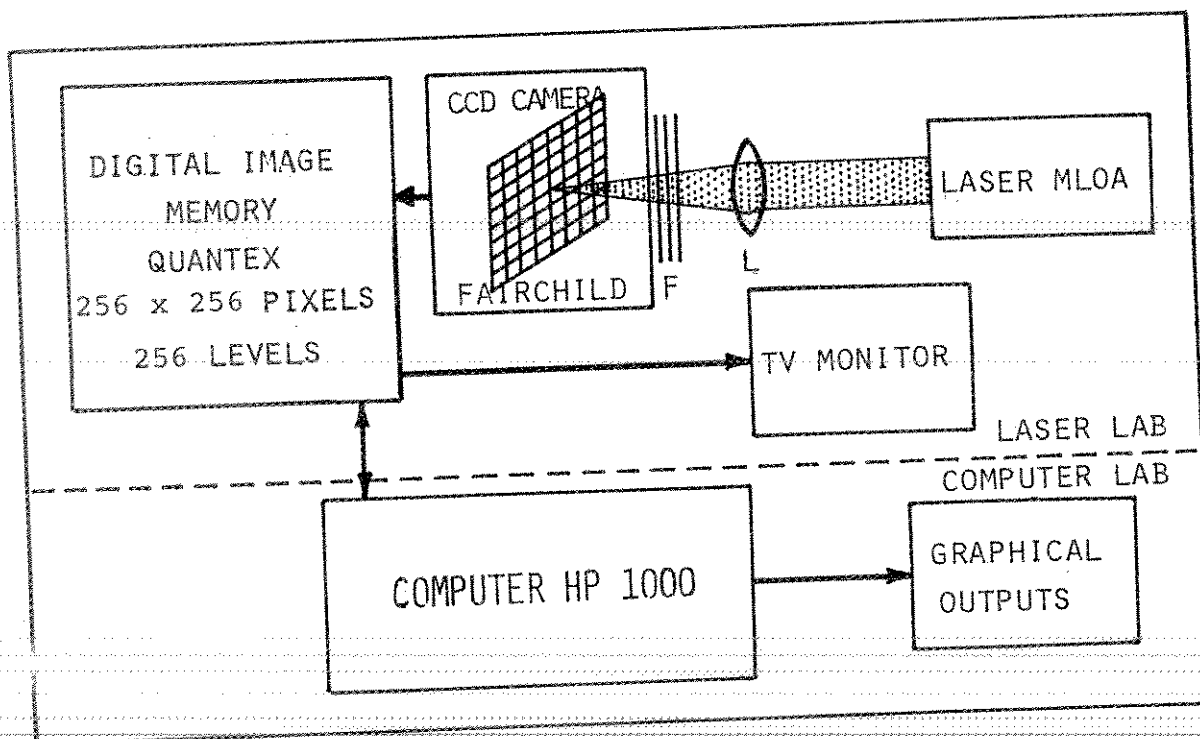
Fig.2. The experimental set up of the farfield beam spatial structure measurements.(F - neutral density filters, L - 2.5 m lens.)
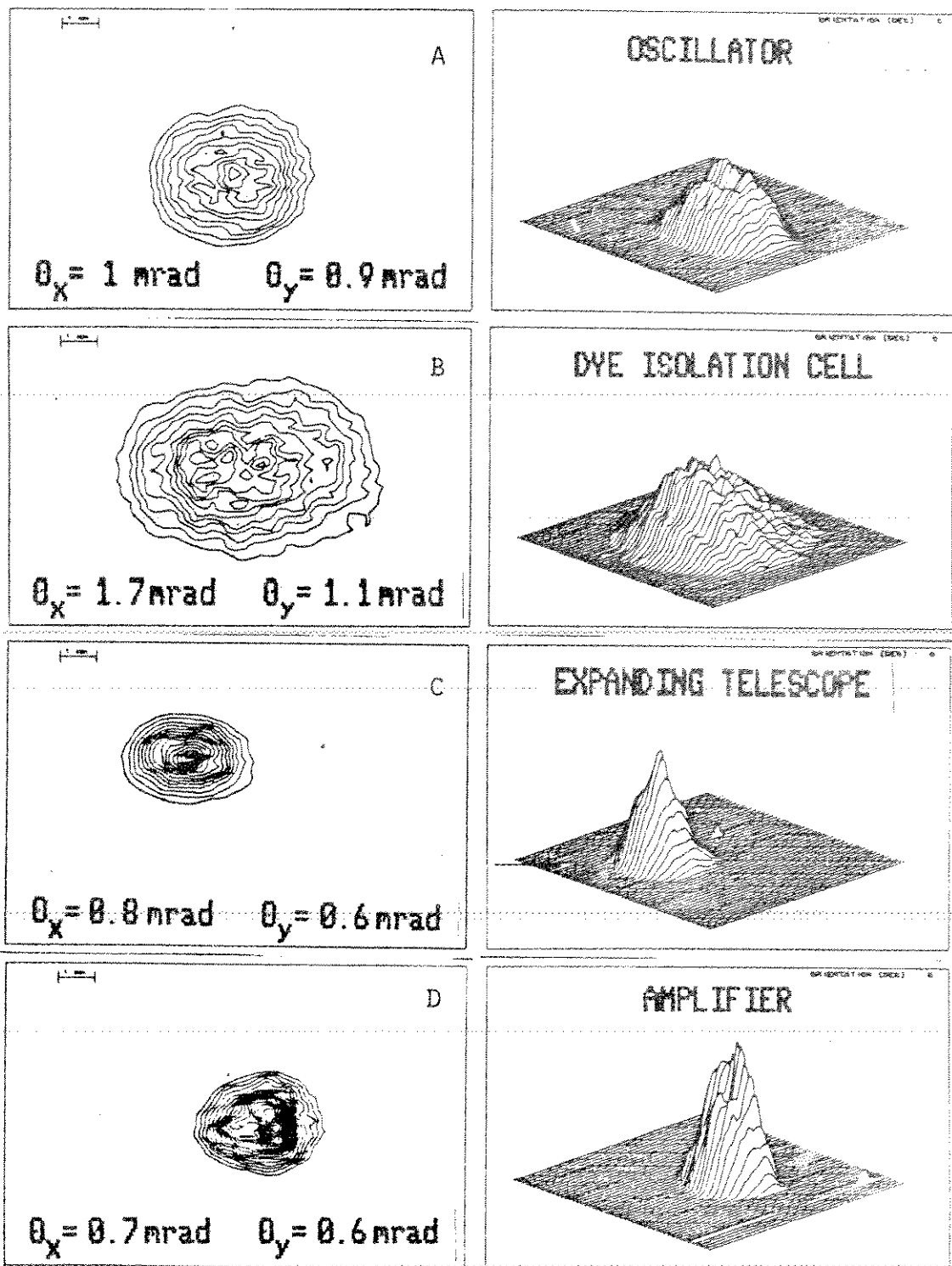
Fig.3. The IR far field beam spatial structure.

Fig.4.

Fig.5.

T = 20°C

T = 24°C

T = 28°C
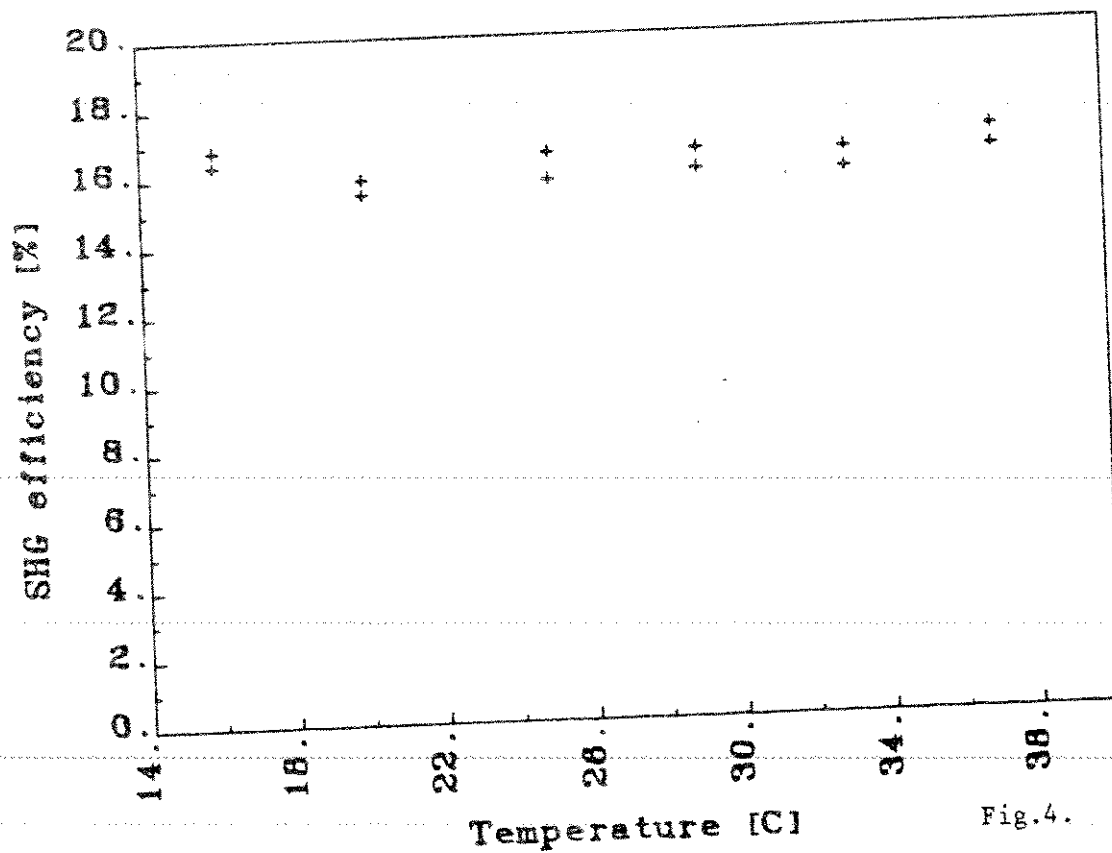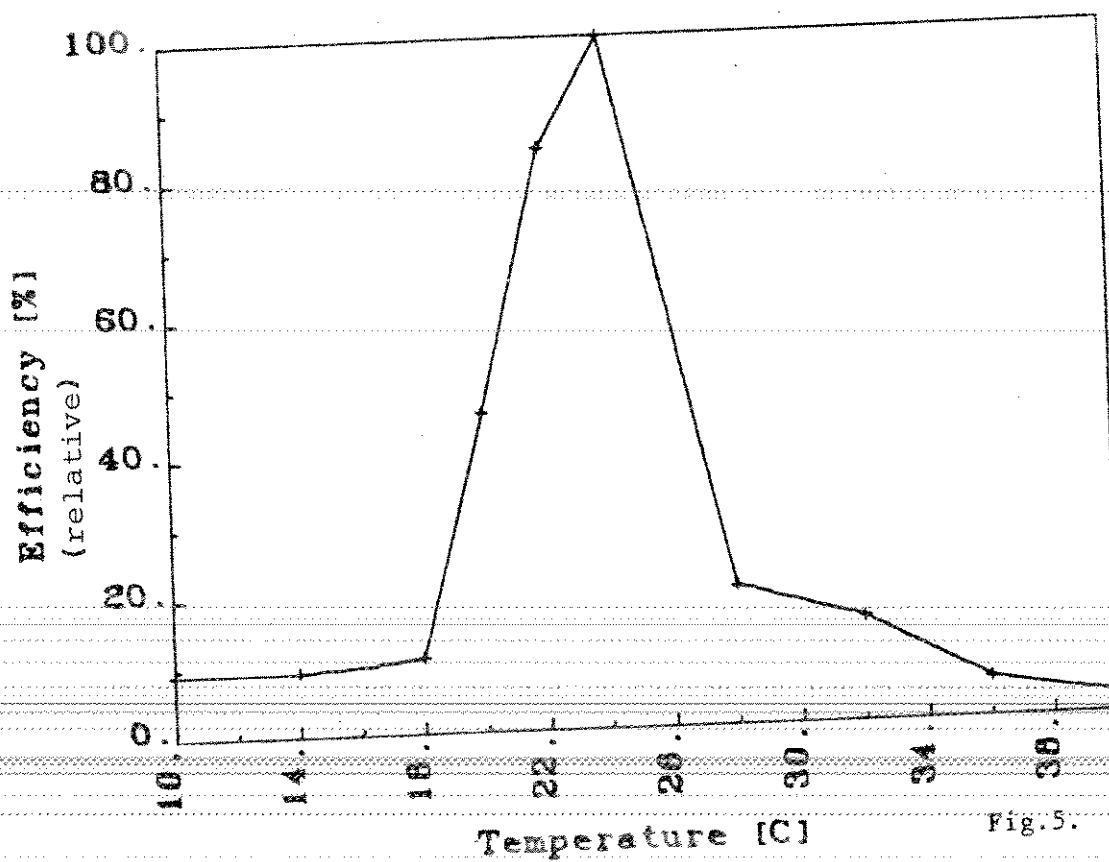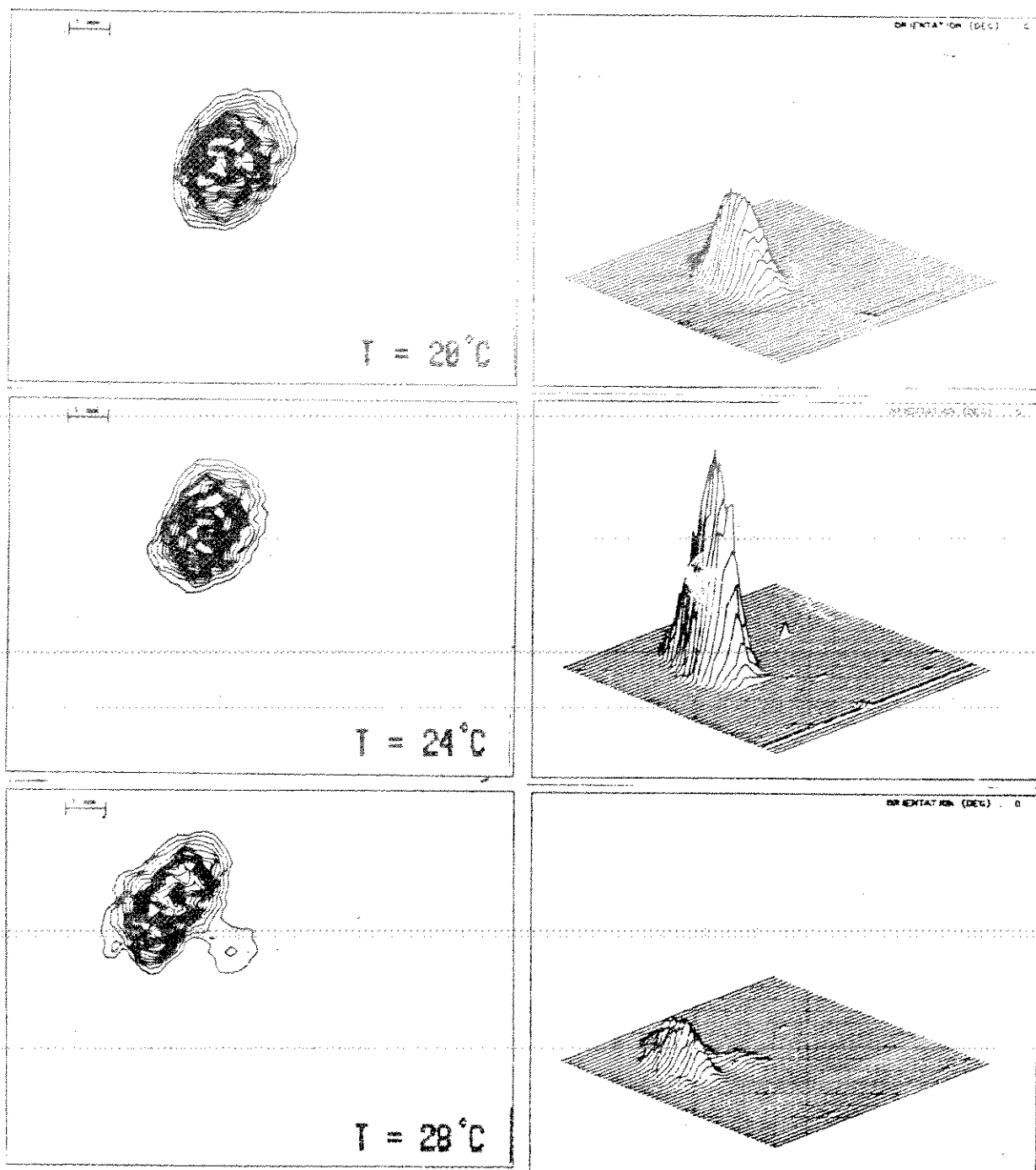
Fig.6. Temperature dependence of the far field SH beam structure.

IR

OSCILLATOR
$\theta_x = 1.00$ mrad $\theta_y = 1.00$ mrad

A

GREEN

SHG - 1 KDP
$\theta_{xy} = 1.01$ mrad $\theta_{yx} = 0.68$ mrad

B

GREEN

SHG - 2 KDP - TANDEM
$\theta_x = 0.48$ mrad $\theta_y = 0.46$ mrad

C

Fig. 7. Aperture effect compensation

SOME SPECIAL REQUIREMENTS
TO LASERS FOR SATELLITE LASER RANGING

L. Jiyu
Wuhan Technical University of
Surveying and Mapping
23 Lo-yu Road, Wuhan
The People's Republic of China

ABSTRACT

When designing or improving an SLR system it will be necessary to take into consideration that which laser should be selected. This paper has given an outline of some special requirements to select a suitable laser.

At present solid-state lasers are used to measure the distances not only between a ground station and the satellite specially equiped with retroreflectors far off several thousand kilometers, but also between a ground station and the moon set by five retroreflectors arrays far off about 380 thousand kilometers. Laser pulses generated by a solid-state laser are not modulated with any way, but used directly to measure the distances. In this case, what requirements are proposed for lasers ? This paper will try to discuss them.

Some Special Requirements to lasers for Satellite Laser Ranging

Liu Jiyu

Wuhan Technical University of

Surveying and Mapping

23 Lo-yu Road, Wuhan

The People's Republic of China

Abstract

When designing or improving an SLR system it will be necessary to take into consideration that which laser should be selected. This paper has given an outline of some special requirements to select a suitable laser.

At present solid-state lasers are used to measure the distances not only between a ground station and the satellite specially equiped with retroreflectors far off several thousand kilometers,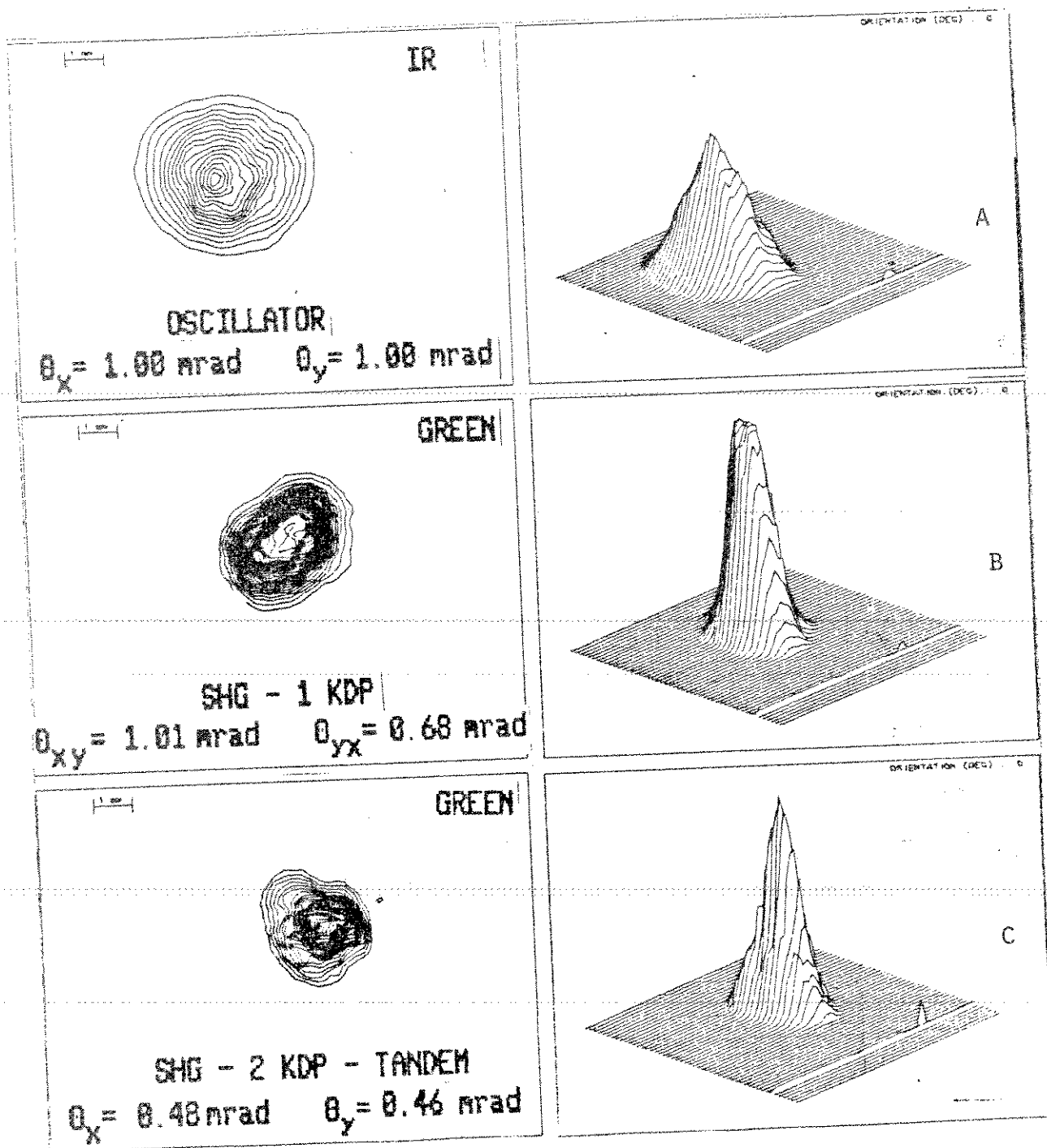 but also between a ground station and the moon set by five retro-reflector arrays far off about 380 thousand kilometers. Laser pulses generated by a solid-state laser are not modulated with any way, but used directly to measure the distances. In this case, what requirements are proposed for Lasers? This paper will try to discuss them.

It is known that the received photons per pulse for SLR systems, N are given as follows:

$$N = \frac{16 E \lambda A_s A_r \tau_t \tau_r \tau^2 \gamma}{\pi^2 h C \delta_t^2 \delta_s^2 D^4} \qquad (1)$$

Where,

E = transmitted energy per pulse, in joule;

λ = laser wavelength, in meter;

A_s = effective area of Satellite-borne retroreflectors, in cm^2;

A_r = effective area of the received objective of a received telescope, in cm^2;

τ_t = transmitter optical transmission;

τ_r = receiver optical transmission;

τ = one-way atmospheric transmission which is a function of zenith distance, site altitude, locality, visibility and wavelength;

γ = reflectivity of the satellite-borne retroreflectors, generally $\gamma = 0.8$;

h = Planck's constant, $h = 6.625 \times 10^{-27}$ erg second;

c = light velocity, in meters/second;

δ_t = full angular divergence of a transmitted laser beam, in arc;

δ_s = reflected laser beam divergence by the satellite-borne retroreflectors, in arc;

D = distance between the ground station and the laser satellite, in cm.

It is seen from the above equation that the parameters, $E\lambda\delta_t$ are dealt with the lasers. How their magnitudes are selected is a problem which laser is designed to satisfy some requirements for an SLR system. Therefore it is very useful to discuss their selections.

Table 1: Lasers used by worldwide SLR systems

country	wavelength	pulsewidth	transmitted power	Repetition rate	Detector type
Australia	532 nm	5-7 nsec	250 mJ	1 pps	2233 Amperex
"	694.3 nm	6 nsec	350 MW	8 ppm	RCA 7265
"	694.3 nm	6 nsec	1 J	12 ppm	RCA 31034
Austria	530 nm	100 ps	100 mJ	up to 10 Hz	
"	694.3 nm	3 ns, 6 ns	2.5 J, 4 J	up to 0.25 Hz	
Brazil	694.3 nm	6 nsec	350 MW	8 ppm	RCA 7265
China	532 nm	5 nsec	20 MW	1 Hz	GDB 49
"	694.3 nm	20 nsec	80 MW	30 ppm	
Cuba	694 nm	30 nsec	50 MW	15 ppm	RCA 8852
Ecuador	694.3 nm	35 nsec	1 J	0.25 pps	FEU-84
Egypt	694 nm	30 nsec	50 MW	15 ppm	RCA 8852
"	694 nm	4 nsec	200 MW	15 ppm	RCA 8852
W-Germany	532 nm	200 pps	0.25 J	4 pps	Varian Static Crossed Field 154
"	539 nm	400 pps	10 mJ	10 Hz	RCA 8850
Finland	694.3 nm	20 nsec	50 MW	4 ppm	RCA C 31034
France	694.3 nm	3 nsec	1.5 J	6 ppm	RCA 31034
"	694 nm	3.5 nsec	3 J	10 ppm	centroid detection
DDR	694.3 nm	20 nsec	0.5 to 1 J	10 ppm	RCAC 34034A
Greece	694.3 nm	25 nsec	4.5 J	8 ppm	RCA 7265
Hungary	694 nm	20 nsec	0.5 J	0.5 Hz	FEU-84
India	694.3 nm	20 nsec	1 J	1 pps	RCA 8852
Japan	694.3 nm	15 ns, 4 ns (with slicer)	0.3 J	0.1 pps	RCA 7265
"	532 nm	200 ps	250 mJ	4 pps	static crossed field
Netherla.	694.3 nm	1.8 nsec	700 mJ	15 ppm	RCA 8852
"	539 nm	400 ps	10 mJ	10 Hz	RCA 8852
Peru	694.3 nm	6 nsec	350 MW	8 ppm	RCA 7265
Poland	694 nm	25 nsec	1.5 J	7 ppm	RCA 8852 with CFD

Table 1 (Continuous)

country	wavelength	pulsewidth	transmitted power	Repetition rate	Detector type
Spain	694 nm	27 nsec	0.7 J	6 ppm	RCA 31034A
Switzerla.	694 nm	17 nsec	1.5 J	0.25 Hz	RCA 7265
United Kingdom	532 nm	150 ps	30 MJ	10 Hz	Varian VPM 152S
USA (Texas)	694.3 nm	3 nsec	0.4 J	20 ppm	RCA 31034A
" "	532 nm	100 ps	0.4 J	10 Hz	RCA 8852
" "	532 nm	100 ps	35 MW	10 Hz	Varian 152S
" (Hawaii)	694 nm	5 nsec	750 mJ	1 pps	56 TVP
" (Colorado)	694 nm	5 nsec	750 mJ	1 pps	56 TVP
" (CA)	694 nm	5 nsec	750 mJ	1 pps	56 TVP
" (GSFC)	532 nm	varied	varied	1 pps	56 TVP
" "	532 nm	5-7 nsec	250 mJ	1 pps	56 TVP
" "	532 nm	0.2-0.4 nsec	250 mJ	1 pps	56 TVP Amperex
" (CA)	532 nm	5-7 nsec	250 mJ	1 pps	56 TVP Amperex
" (GSFC)	532 nm	0.2-0.4 nsec	250 mJ	1 pps	56 TVP Amperex XP2233
" (Maui)	532 nm	500 ps	0-6 J	3 Hz	Amperex XP2233
USSR	694.3 nm	20 nsec	50 MW	0.7 Hz	FEU-79
"	694.3 nm	25 nsec	1 J	0.33 Hz	FEU-84

On the basis of the materials published by the Fourth International Workshop on Laser Ranging Instrumentation held at the University of Texas in Austin, Texas USA, October 12-16, 1981 the essential specifications of the lasers operating in worldwide SLR systems are shown in the Table 1. The used laser wavelengths are of three types of 6943 Å, 5320 Å and 5390 Å, corresponding with three laser medium of ruby, Nd:YAG and Nd:YAP crystal. The longer laser wavelength used is to the benefit of detections with the view of the transmission traveled in the atmospheric layer (see Table 2). Under the condition of the smallest zenith distance there is not greater difference between

Table 2: Atmospheric transmission at different wavelengths and zenith distances, from Mastrocinque

λ (nm)	$\tau(0°)$	$\tau(60°)$	$\tau(70°)$
760	0.79	0.63	0.50
694.3	0.77	0.58	0.45
532	0.67	0.45	0.30
380	0.44	0.20	0.09

atmospheric transmission at different wavelengths. However, the smaller the elevation is, the greater the transmission difference gets. For example, the atmospheric transmission of 6943 Å laser will be 50 % higher than that of 5320 Å laser obtained with a second harmonic generator (SHG) when the elevation is equal to 20°. It is known that the SHG halves the wavelength of 1064 nanometers generated by Nd:YAG laser to 532 nanometers which is in the visible region of the spectrum. If there should be any photoelectronic conversion device which is of higher efficiency of quantum for a infrared laser it would be of great advantage for SLR systems to directly use the laser beam generated by the laser system without

SHG, such as 1064 nm laser falling within an atmospheric window. When omiting the SHG for which maximum conversion efficiency is up to 30 percent (energy) the latter is equivalent to increase the transmitted energy of about 70 percent. On the other hand, it will be seen from equation (1) that the received photons varies as the laser wavelengths. Under the condition of the same parameters the number of the received photons is increased with an increased wavelength. It will be possible to execute normal SLR with the smaller transmitted energy produced by a simplified laser.

If there is any significant drift for the laser wavelengths this will produce three bad effects. First is a transmission decrease for a telescope. It is known that the coatings of all optical components are compatible with a certain operation wavelength. The greater the drift of the laser wavelength is, the smaller the transmission for a transmitted laser beam gets. Second is an attenuation increase for a narrowband filter. In order to heighten the signal-to-noise ratio a narrowband filter is used in a receiver based on PMT. Due to a very narrow FWHM, such as that of 1 ± 0.2 Å, the attenuation of the narrowband filter for the returned laser will be greatly increased when there is any greater drift (see Fig.). For example, when the drift of laser wavelengths is equal to ± 0.5 Å the transmission gotten through the narrowband filter will be decreased to 50 percent. Third is a reduction of the conversion efficiency from a light pulse to an electronic one. The peakconversion for a photocathode is compatible with a certain wavelength. Due to the drifted wavelength the conversion efficiency can not be impinged in the peak region. It will be seen from these that the stability of the laser wavelength is very important to insure the optimal operation for SLR systems. The spectral line stability should be better than a few subangstroms.

It will be seen from Table 1 that in 44 lasers used by worldwide SLR systems the minimal transmitted energy is 10 millijoules, the maximum 4.5 joules; the minimal pulsewidth is 100 picoseconds,

transmission

S

P

1Å

laser wavelength
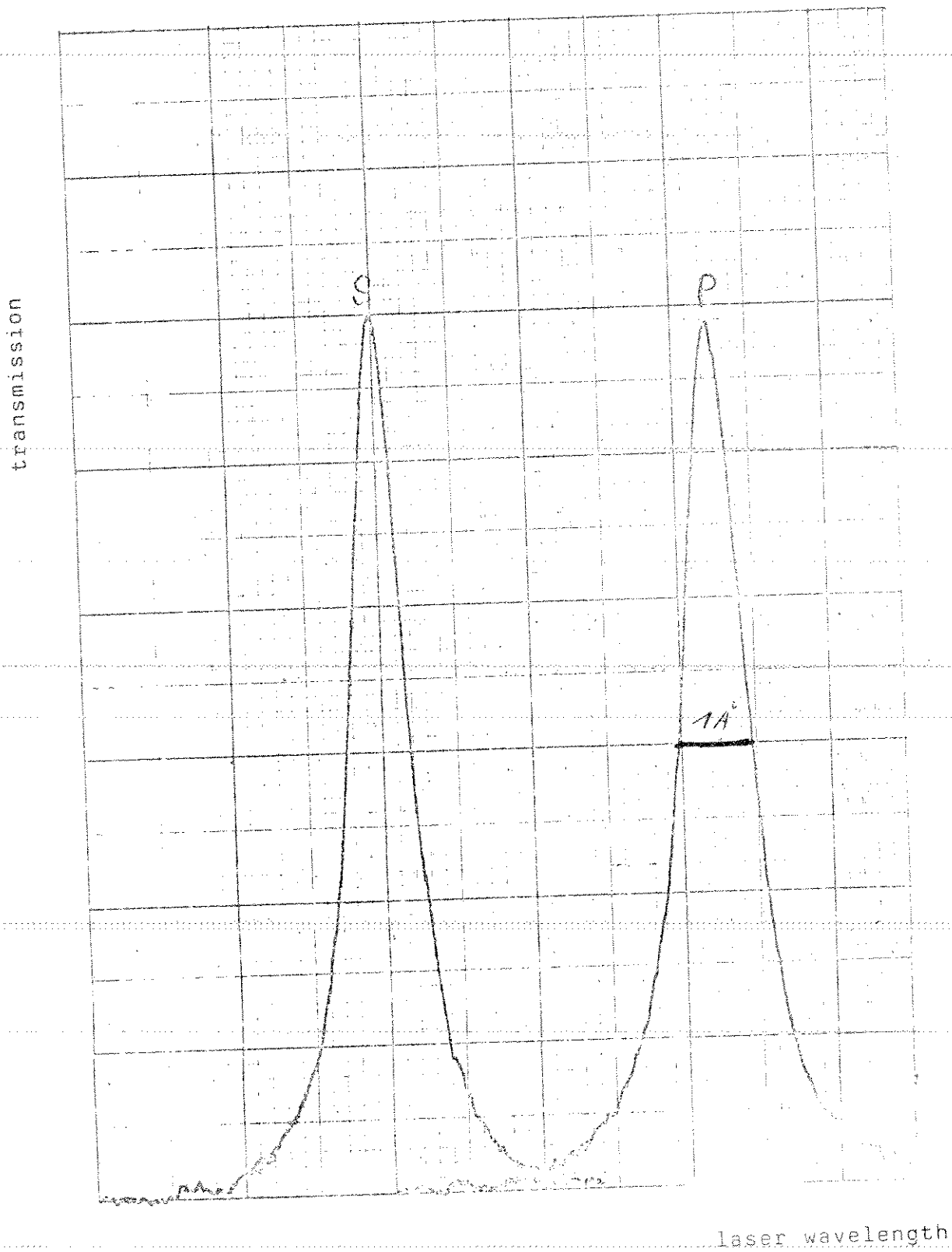
Transmission of double peak polarized interference filters
produced by Daystar filter corporation, California, USA

the maximum 35 nanoseconds. It was pointed out that the more narrow
the laser pulsewidth, the smaller the pulsewidth error [Liu, 1985].
In practice the relationship was also found with constraining the
laser pulsewidth. For example, the pulsewidth was constrained from
25 nsec to 6 nsec by means of a pulse chopper in an SAO SLR system
so that the ranging accuracies increased to at least 50 percent
[Tapley, et al, 1982]. From the following equation it can be
demonstrated:

$$M_W = \frac{k_p \, \tau_p}{\sqrt{N_r}} \tag{2}$$

Where,

M_W = pulsewidth error;

τ_p = FWHM of a laser pulse;

N_r = number of received photoelectrons;

k_p = coefficient depending on different detection.

However, to use the pulse chopper for a narrow laser pulsewidth is
a temporary improvement means. Due to its reject for a sizable frac-
tion of the laser energy it is not efficient. An essential and effi-
cient means is to employ the new laser which can not only generate
laser pulses as short as 30 psec, but also operate in a pure funda-
mental TEM_{00} mode. The latter can produce the smallest beam diver-
gence, the highest power density, and, hence, the highest brightness.
Furthermore, the radial intensity profile is uniform and uniphase
[Koechner, 1976]. The experiment by GSFC demonstrated that the re-
quirements can be satisfied essentially when using modelocked Nd:YAG
lasers. Their repeatability and rangemap measurements have shown
less than 2 cm peak-to-peak variation in 100 point mean. The repea-
tability and rangemap measurements for PTM Q-switched and Q-switched
lasers were of more than 6 cm peak-to-peak variation in 100 point
mean [Degnan and Zagwodzki, 1982]. It will be seen from the above

that modelocked Nd:YAG (or YAP) lasers should be substituted for Q-switched ones. The latter has also other problem leading to a wavefront error. Its source and magnitude have been discussed in another paper [Liu, 1985]. For at least decreasing the wavefront error SLR systems do not employ also the Q-switched lasers, but the modelocked ones.

From what has been said above, we know that it is suitable for lasers to be able to generate the following pulses:

- stable wavelength laser pulses, so as to insure the optimal operation for SLR systems. If there should be any device which can effectively detect infrared lasers it would be very benefi- cial to use longer laser wavelength for SLR;

- higher repetition laser pulses, so as to acquire more ranging data in one satellite pass; but due to limitations of thermal transients which disturb the fine balance within the optical resonator and high peak power nonlinear effects which can lead to the irreversible breakdown of materials subnanosecond laser pulses are limited to about 20 pps repetition rate [Hyde and White- head, 1982];

- short sharp laser pulses, so as to improve the accuracy for mea- surements to the time interval between a transmitted and returned laser pulse;

- powerful peak laser pulses. so as to be able to measure the dis- tances not only to the satellite-borne retroreflectors, but also to the moon-borne retroreflector array;

- purer fundamental laser pulses, so as to obtain an uniform and uniphase intensity profile for precise SLR.

References

[1] G. Mastrocinque, Feasibility of Satellite Tracking with a
        Dual-wavelength Laser Ranging System
        ESA Journal, 1985, Vol. 9, pp 273-286

[2] Liu Jiyu, Satellite Laser Ranging Errors

[3] W. Koechner, Solid-state Laser Engineering, 5.1.9 Mode
        Selecting techniques
        Springer-Verlag, Berlin, 1976

[4] J.J. Degnan and T.W. Zagwodzki, A Comparative Study of
        Several Transmitter Types for precise Laser Ranging
        Proceedings of the Fourth International Workshop on
        Laser Ranging Instrumentation, published by the
        Geodetic Institute, University of Bonn, 1982,
        pp. 241 - 250

[5] R.L. Hyde and D.G. Whitehead, Some Problems of Short Pulse,
        Low Energy, High Repetition Rate Lasers
        Applied to Satellite Ranging Systems
        Proceedings of the Fourth International Workshop on
        Laser Ranging Instrumentation, published by the
        Geodetic Institute, University of Bonn, 1982,
        pp. 251 - 259
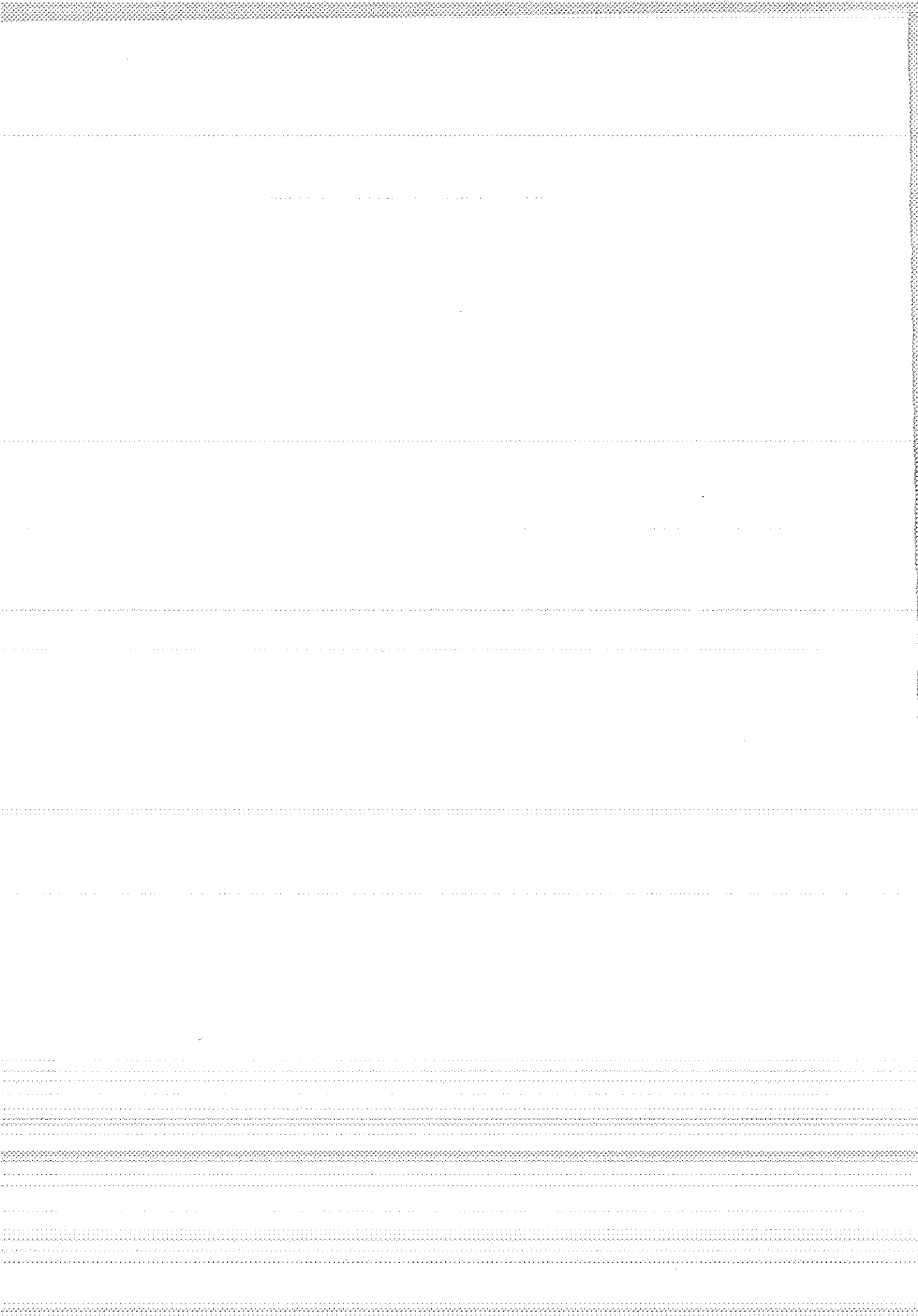
ANALYSIS AND PERFORMANCE OF A PASSIVE
POLARIZATION TELESCOPE COUPLING SWITCH
FOR LUNAR LASER RANGING

S.R. Bowman, J.R. Rayner, C.O. Alley
Department of Physics and Astronomy
College Park, MD 20742

Telephone (301) 454 3405

ABSTRACT

A passive polarization switch is an attractive way to couple a laser transmitter and receiver to a telescope because it is so simple. However, few laser ranging stations have implemented such a switch because of concern about depolarization of the beam by the target. Here we show that the amount of depolarization is less than one might expect by considering the case of the Apollo lunar reflectors.

ANALYSIS AND PERFORMANCE OF A PASSIVE POLARIZATION TELESCOPE COUPLING SWITCH FOR LUNAR LASER RANGING

S. R. Bowman, J. R. Rayner, C. O. Alley
Department of Physics and Astronomy
College Park, MD 20742

Telephone (301) 454-3405

ABSTRACT

A passive polarization switch is an attractive way to couple a laser transmitter and receiver to a telescope because it is so simple. However, few laser ranging stations have implemented such a switch because of concern about depolarization of the beam by the target. Here we show that the amount of depolarization is less than one might expect by considering the case of the Apollo lunar reflectors.

INTRODUCTION

In order to separate the transmitted from the returned beams, some sort of switch is required. Most laser ranging systems incorporate a rotating mirrored chopper wheel for the switch. While this approach is conceptually simple it can lead to some practical problems. The wheel must spin stably while staying in phase with a high repetition rate laser. The limited extinction ratio between the two paths requires some additional blocking mechanism. Also, for realistic spin rates this type of switch is too slow for terrestrial ranging.

For the Goddard/Maryland Lunar Ranging System, a passive polarization switch was chosen.[1] It has the advantage of being very simple to implement, consisting of only a thin film Brewster angle polarizer and a zero order quarter wave plate. It has the disadvantage of losing some return light due to depolarization, but this is more than compensated for by its reduction of the noise by a factor of two. This section examines the efficiency of such a switch for lunar ranging.

DEPOLARIZATION FROM APOLLO REFLECTORS

After the second harmonic generator a half wave plate is used to rotate the linear polarization to the vertical, Figure 1. The "S" polarization is reflected off a thin film polarizer and passes through a zero order quarter wave plate into the telescope. (The zero order plate is needed to prevent temperture variation from affecting the polarization state.) Returning light of the correct polarization will become "P" polarized after a second trip through the quarter wave plate. Using Jone's calculus the polarization state can be computed each step of the way.[2]

Define a coodinate system on the optical table as shown in
Figure 2. Transmission of the "S" polarization through the λ/4
plate gives a polarization state

$$U_s = \frac{1}{2} \begin{pmatrix} 1+i \\ 1+i \end{pmatrix} .$$ (1)

Multiple reflections off the telescope mirrors will change the
polarization state. However measurments of this effect show it
to be small. A helium neon laser with an arbitrarily oriented
linear polarization was transmitted through the telescope. The
attenuation of the transmitted beam by a crossed linear
polarizer was measured at many telescope positions. The
linearly polarized intensity was found to be preserved to
within 5%. Since this change is small and is reversed upon
returning through the telescope, it is ignored here. It cannot
be ignored, though, that the polarization axis will rotate as
the telescope tracks in azimuth. This effect combined with the
changing orientation of the moon as it passes overhead will be
accounted for by a rotation transformation of the corner cube
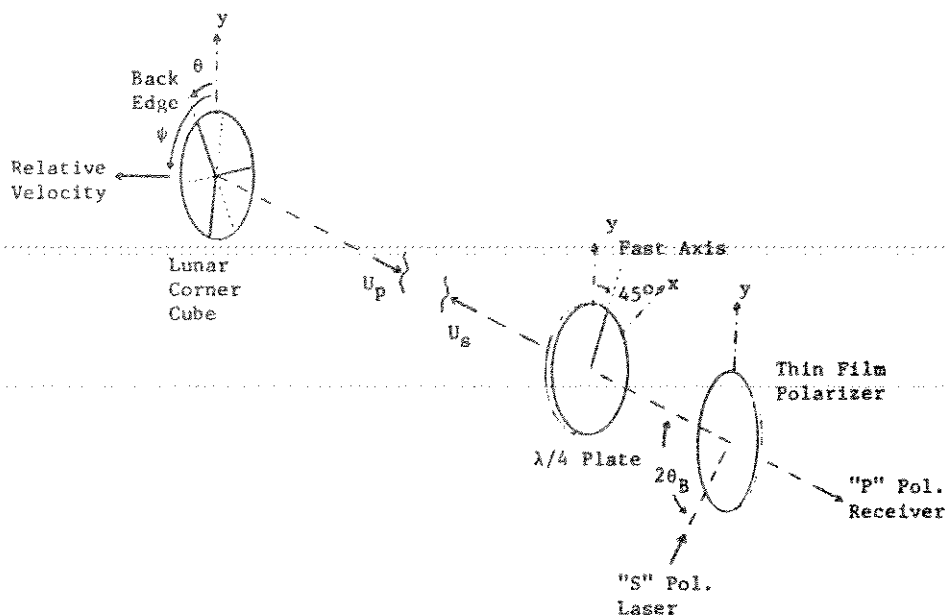array.

PASSIVE POLARIZATON SWITCH

FIGURE 1

What happens to the polarization of a beam when reflected from a total internal reflection corner cube was first studied by E.R. Peck.[3] R.F. Chang et al.[4] extended the analysis to include far field diffraction of linear polarization from a corner cube. In a similar calculation, the Fraunhofer diffraction pattern for normally incident, circularly polarized light from a corner cube can be determined. Then the efficiency of the passive polarization switch can be evaluated once the velocity aberration effect is accounted for.

Upon reflection from a lunar corner, the incident beam is broken up into six wedge shaped beams. In general, each of these beams will have a different polarization. These six polarization states, $\underline{V}^n$, can be calculated from the equation

$$(\underline{V}^n_x, \underline{V}^n_y) = \underset{\approx}{C}^n \cdot \underline{U}_s. \tag{2}$$

The authors mentioned above have calculated the polarization matrix $\underset{\approx}{C}^n$ consistent with the coordinates choosen here for the case of one back corner edge parallel to the "y" axis.

$$\underset{\approx}{C}^1 = \xi \underset{\approx}{1} + \sqrt{1/2}\ \eta\ \underset{\approx}{\sigma}_z + \zeta\ \underset{\approx}{\sigma}_y + \sqrt{3/2}\ \eta\ \underset{\approx}{\sigma}_x$$

$$\underset{\approx}{C}^2 = \xi \underset{\approx}{1} + \sqrt{2}\ \eta\ \underset{\approx}{\sigma}_z + \zeta\ \underset{\approx}{\sigma}_y$$

$$\underset{\approx}{C}^3 = \xi \underset{\approx}{1} + \sqrt{1/2}\ \eta\ \underset{\approx}{\sigma}_z + \zeta\ \underset{\approx}{\sigma}_y - \sqrt{3/2}\ \eta\ \underset{\approx}{\sigma}_x \tag{3}$$

$$\underset{\approx}{C}^4 = \xi \underset{\approx}{1} + \sqrt{1/2}\ \eta\ \underset{\approx}{\sigma}_z - \zeta\ \underset{\approx}{\sigma}_y - \sqrt{3/2}\ \eta\ \underset{\approx}{\sigma}_x$$

$$\underset{\approx}{C}^5 = \xi \underset{\approx}{1} - \sqrt{2}\ \eta\ \underset{\approx}{\sigma}_z + \zeta\ \underset{\approx}{\sigma}_y$$

$$\underset{\approx}{C}^6 = \xi \underset{\approx}{1} + \sqrt{1/2}\ \eta\ \underset{\approx}{\sigma}_z - \zeta\ \underset{\approx}{\sigma}_y + \sqrt{3/2}\ \eta\ \underset{\approx}{\sigma}_x$$

In terms of the total internal reflection coefficients r_s and r_p

$$\xi = \frac{1}{16}\ (r_s + r_p)[\ 3(r_s + r_p)^2 - 2\ (r_s - r_p)^2\ ]$$

$$\eta = \frac{\sqrt{2}}{16}\ (r_s + r_p)^3 \tag{4}$$

$$\zeta = -i\ \frac{\sqrt{3}}{16}\ (r_s + r_p)^2(r_s - r_p).$$

For an arbitrary azimuthal orientation of the corner, the matrix $\underset{\approx}{C}^n$ must be rotated about the "z" axis. It is easy to see that only the "x" and "z" Pauli matrix components are affected by a rotation of angle θ. To transform $\underset{\approx}{C}^n$ to $\underset{\approx}{C}^n(\theta)$, one only need substitute

$$\underset{\approx}{\sigma}_x(\theta) = \begin{pmatrix} -\sin 2\theta, \cos 2\theta \\ \cos 2\theta, \sin 2\theta \end{pmatrix} \quad \text{and} \quad \underset{\approx}{\sigma}_z(\theta) = \begin{pmatrix} \cos 2\theta, \sin 2\theta \\ \sin 2\theta, -\cos 2\theta \end{pmatrix}. \tag{5}$$

Combining the last few equations gives the polarization state vectors, $\underline{V}^n$, for the six normally reflected beams from an azimuthally rotated total internal reflection corner cube. In order to evaluate the efficiency of the polarization switch, the components of each $\underline{V}^n$ that are transmitted and rejected must be found. Transforming back through the $\lambda/4$ plate shows that:

$$\underline{U}_p = \tfrac{1}{2} \begin{pmatrix} 1 & + & i \\ 1 & - & i \end{pmatrix} \tag{6}$$

is the transmitted polarization state. The components of the $\underline{V}^n$'s in the $\underline{U}_p$ and $\underline{U}_s$ directions are

$$\gamma_p^n = \underline{V}^n \cdot \underline{U}_p = -\xi + \zeta \quad \text{(for odd n)}$$
$$= -\xi - \zeta \quad \text{(for even n)}$$

and

$$\gamma_s^n = \underline{V}^n \cdot \underline{U}_s = \eta \, \delta_n \, e^{i2\theta} , \tag{7}$$

where the complex numbers δ_n are given in Table (1).

The normalized reflected electric field from the nth subaperture of the jth corner cube in the array can now be written as

$$\underline{A}_j^n = [\; \gamma_p^n(\theta_j) \; \underline{U}_p + \gamma_s^n(\theta_j) \; \underline{U}_s] \; \exp(i\Delta_j) . \tag{8}$$

The phase Δ_j is the overall optical delay for the jth corner. For even slight variations in the physical dimensions or temperatures of the corners, the optical delay will vary over one wavelength. For this reason the following analysis assume Δ_j to be random.

Records of the construction of the lunar corner reflector packages show that all the corners in the arrays were carefully oriented alike.[5] Therefore, the subscript on θ_j can be dropped.

After propagating back from the moon, the beam from each of the corner cubes will be spread by diffraction. For the jth corner the field component in the U_p direction at a point Q will be

TABLE 1

n	δ_n
1	$\sqrt{3/2} - i/2$
2	$+i$
3	$-\sqrt{3/2} - i/2$
4	$-\sqrt{3}/2 + i/2$
5	$+i$
6	$\sqrt{3}/2 + i/2$

$$u_j^p(Q, \theta) = \frac{1}{\pi a^2} \exp(i\Delta_j) \int_0^a \rho d\rho \int_0^{2\pi} \gamma_p(\phi,\theta) e^{-ik\rho\sin\alpha\cos(\phi-\psi)} d\phi \ . \quad [8]$$

(9)

Here (ρ,ϕ) are polar coordinates on the corner aperture and (α,ψ) are the angles locating the point Q relative to the center of the diffraction pattern. Dividing by the area of the corner, πa^2, normalizes the amplitude for $\alpha = 0$. Rewriting the ϕ integral in terms of the six subapertures gives

$$u_j^p(Q,\theta) = \frac{1}{\pi a^2} \exp(i\Delta_j) \sum_{n=1}^6 \gamma_p^n(\theta) \int_0^a \rho d\rho \int_{\theta+(2n+1)\pi/6}^{\theta+(2n+3)\pi/6} \exp[-ik\rho\sin\alpha\cos(\phi-\psi)] d\phi$$

(10)

With the definition of $x = ka\sin\alpha$ and the use of the Bessel series expansions

$$e^{-iy\cos\beta} = J_0(y) + 2\sum_{\ell=1}^\infty (-i)^\ell J_\ell(y)\cos(\ell\beta)$$

and
$$\int_0^x y J_\ell(y) dy = 2\ell x \sum_{m=0}^\infty \frac{(\ell + 2m + 1)}{(\ell + 2m + 2)(\ell + 2m)} J_{\ell+2m+1}(x)$$

(11)

the amplitude component becomes

$$u_j^p(Q, \theta) = \frac{1}{3x} \exp(i\Delta_j) J_1(x) \sum_{n=1}^6 \gamma_p^n$$

$$+ \frac{8}{\pi x} \exp(i\Delta_j) \sum_{\ell=1}^\infty (-i)^\ell \sin(\ell\pi/6) \sum_{n=1}^6 \gamma_p^n \cos\{\ell[\pi(n+1)/3 + \theta - \psi]\}$$

$$* \sum_{m=0}^\infty \frac{(2m+\ell+1)}{(2m+\ell)(2m+\ell+2)} J_{2m+\ell+1}(x) \quad (12)$$

If the laser pulse duration is long enough, the fields from all of the N corners will superimpose. In the approximation that N is large, the transmitted intensity will be

$$I^p(Q, \theta) = \left| \sum_{j=1}^N u_j^p \right|^2 \approx N|u_j^p|^2. \quad (13)$$

Likewise, the rejected intensity will be

$$I^s(Q, \theta) = \left| \sum_{j=1}^N u_j^p \right|^2 \approx N|u_j^p|^2. \quad (14)$$

The polarization switch efficiency can now be written as

$$e(Q, \theta) = |u^p|^2 / [|u^p|^2 + |u^s|^2] \quad (15)$$

where the subscript j is now superfluous.

For small x, the J_1 term dominates the expression for u^p and the efficiency approached unity. Realistically though, the diffraction pattern is never centered on the receiver. It was shown earlier that

$$4.0 \leq |\alpha| \leq 7.3 \text{ microradians.} \quad (16)$$

as a result of velocity aberration. Figure 2 shows the switch

POLARIZATION SWITCH EFFICIENCY
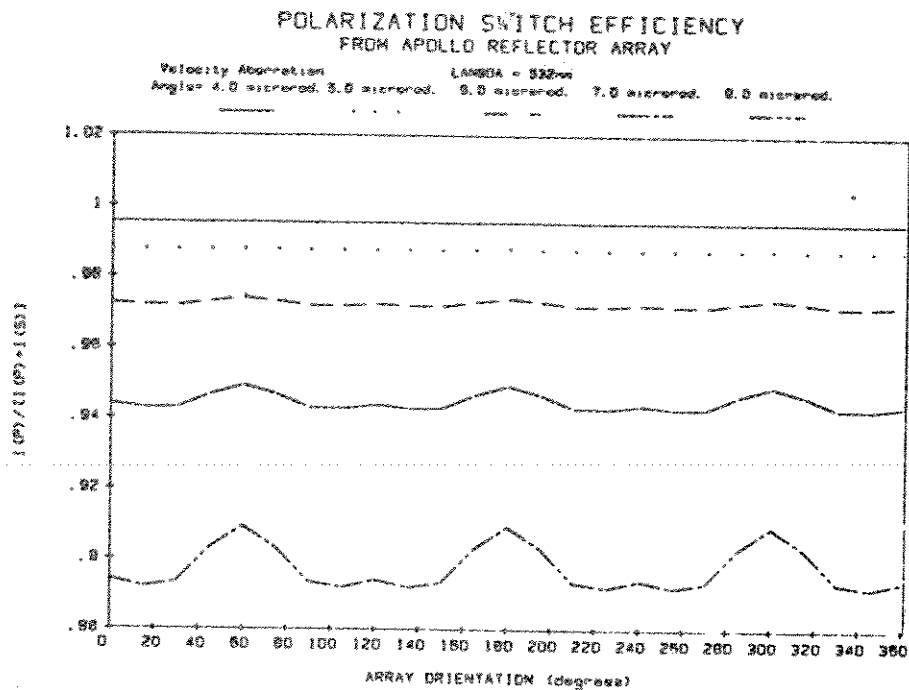FROM APOLLO REFLECTOR ARRAY

FIGURE 2

efficiency for several intermediate velocity aberration
angles. It is clear from these curves that the depolarization
is a weak function of the corner array orientation, θ~ψ. More
importantly though, the passive switch efficiency is better
than 90% for all cases.

From the example calculation for lunar targets one would
expect the depolarization losses to increase for other targets
as the velocity aberration increases, although the exact
calculation depends on the details of the targets structure.
This means that the highest losses would be expected for the
lowest satellites since they have the highest relative
velocity. In practice, the passive polarization switch has
been found to work very well for LAGEOS, BE~C, and GEOS~A.

CONCLUSIONS
Passive polarization switches are a simple, efficient way
of coupling the laser and reciever to a laser ranging
telescope. For lunar ranging operations, depolarization losses
of less than 10% can be expected. Additional advantage is
gained in noise reduction by the filtering of the unwanted
polarization.

REFERENCES

1. The idea of using a polarization switch for coupling the laser and detector was originally suggested by Professor Douglas G. Currie about 1976. Its first use was reported in: C.O. Alley et al., "Experimental Range Measurements at the Single Photo-Electron Level to the GEOS-A and BE-C Satellites," Third International Workshop on Laser Ranging, Lagonisi,Greece, May 1978.

2. R.C. Jones, "A New Calculus for the Treatment of Optical Systems," J. Opt. Soc. Am., 31 (1941), 488.

3. E.R. Peck, "Polarization Properties of Corner Reflectors and Cavities," J. Opt Soc. Am., 52 (1962), 253.

4. R.F. Chang et al., "The Far Field Diffraction Pattern for Corner Reflectors with Complex Reflection Coefficients", J. Opt. Soc. Am., 61 (1971), 431.

5. Laser Ranging Retro-Reflector Array for the Early Apollo Scientific Experiment Package, Final Report to Aerospace Systems Division The Bendix Corporation, Arthur D. Little, Inc., Cambridge, Mass., June 30, 1969.

6. M. Born and E. Wolf, Principles of Optics, (New York: Pergamon Press, 1985), p. 394.

AN ACCURATE TEST OF THE AZIMUTH AXIS OF A 1.2M ALT-AZ TELESCOPE MOUNT FOR THE LUNAR LASER RANGING AND THE ANALYSIS OF THE RESULTS

H. Feng, Y. Xiong, Y. Zhang, J. Wang
Yunnan Observatory
Academia Sinica
P.O Box 110
Kunming - China -

Telephone 729 46
Telex 64040 YUOBS.FN

ABSTRACT

The wobble of the azimuth axis of a 1.2m Alt-Az telescope mount for the Lunar Laser Ranging is measured by means of an accurate method. The systematic error is separated out and the random wobble is found to be about 0".08. The relation between the systematic error and the structure of the mount is also given in this article.

I. Introduction

Because of the long distance between the Earth and the Moon, the lunar laser ranging works approximately to the threshold of detection for the current laser ranging technology. In addition, the aim actively pursued by all the lunar laser ranging stations today is to make the lunar laser ranging by means of the absolute pointing of a telescope so as to increase in the number of days for the ranging. But the necessary condition is that the telescope should have highly accurate pointing. However, the pointing is based on the stability of the axis system. It is known that because of the error in the level adjustment or mechanical faults of the mount even the effects of the environments, the azimuth axis of the mount can not coincide with the direction of the plumb line of the station. The deviation consists of the systematic error and random wobble. Our aim is to seek for an accurate testing method, analyse the measured data, extract the systematic error from them and make an exactly quantitative estimate of the random wobble. It is hopeful to make compensation for the systematic error extracted when a computer is used to correct the telescope pointing. Moreover, some very interesting details related to the structure of the telescope mount are also found as the systematic error is analysed.

II. The Measuring Method

The most direct method for determining the deviation of the azimuth axis from the local plumb line is that the shift of a fine bubble, which is put at the top of the azimuth axis, is observed when the mount turns around the axis. Our measuring method still follows this principle, but the measurement accuracy is greatly improved.

The Talcott level used on the Zeiss transit instrument is adopted and one of the graduations is measured to be 1.17 arcsec (at about $20°$ C). The level bubble is fixed on an adjustable support which is installed at the top of the azimuth axis. Two small measuring telescopes, each with a micrometer, are used to determine the position of either end of the bubble, respectively. As two measuring telescopes may be pointed to the targets within a short range and one graduation of the bubble may be equivalent to 130 divisions on the micrometer. And it is easy to estimate the readout of 1/5 division on the micrometer. In this way the readout resolution may be up to 1/500 arcsec. Of course, the actual measurement accuracy can not be so high, which is limited by the factors such as the sighting accuracy, the manufacture precision of the bubble, the effects of the environment and so on.

When the measurement is carried out the bubble is firstly put in the direction paralleled to the altitude axis. As the mount is turned at $10°$ around the azimuth axis, the positions of the two ends of the bubble are determinated by the micrometers separately and the mean of the two readouts represents the position of the center of the bubble. Then place the bubble in the direction perpendicular to the altitude axis

and repeat the steps of the measuring method mentioned above.
    We have made the measurement of 46 circles in all (with
36 measuring points and 37 readouts per circle). The measured
data of the last 20 circles are used for the quantitative
calculation and analysis. When the measurements of half of
the 20 circles are made, the bubble is parallel with the
altitude axis,and for the other half is perpendicular to the
altitude axis.

III. The Results and their Analyses

    When the measured results are shown graphically, it is
not difficult to find that the systematic error is evidently
included in the results and there appears good repeatability
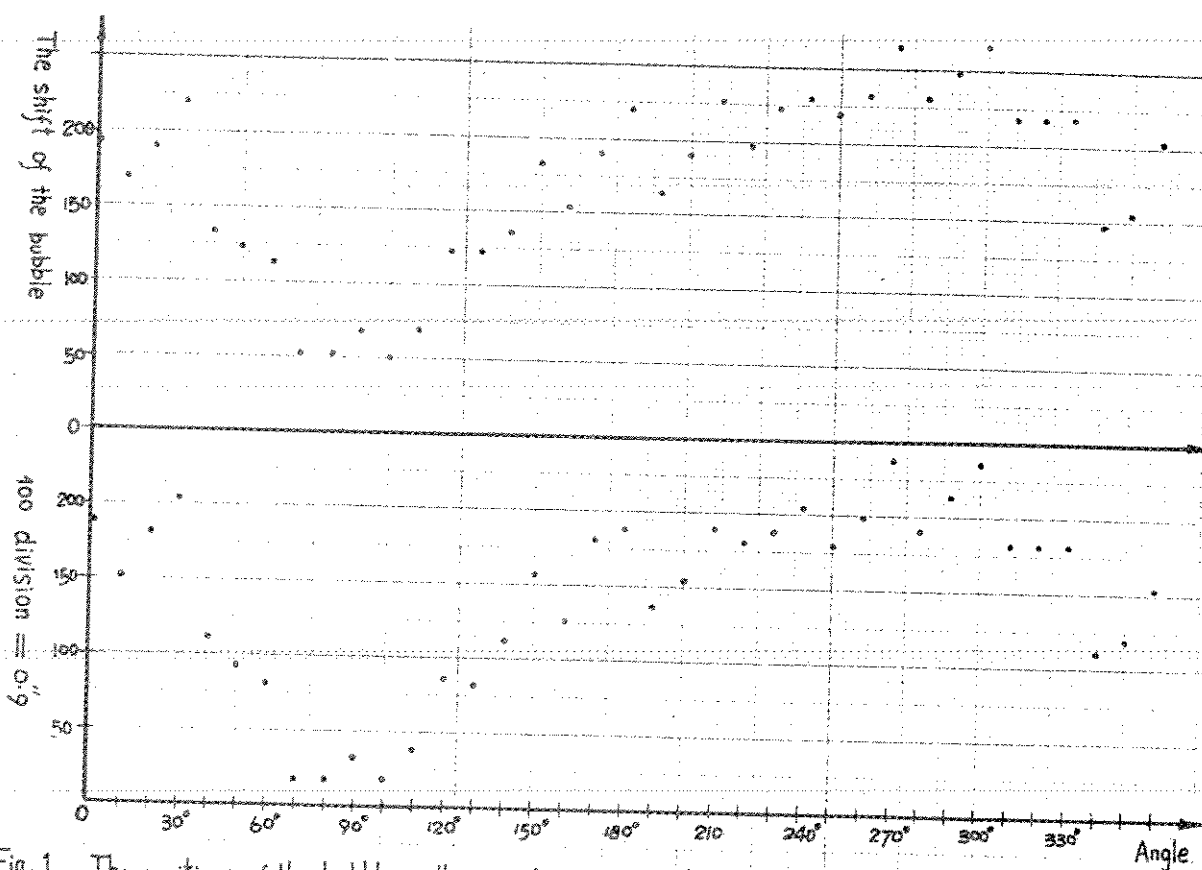between the circles (Fig.1).

Fig.1. The positions of the bubble as the mount is turned at 10° around the azimuth axis

Using a trigonometric polynominal to fit the data, we can
obtain the corresponding harmonic components. The first harmo-
nic mainly originates from the level adjustment error of the
mount,while the phases of the maxima of the third harmonic
just correspond to the three bearing points of the mount,res-
pectively. And it is of interest to note that the results
also contain a twelveth harmonic,of which the amplitude is
considerable and stable. The twelveth harmonic corresponds
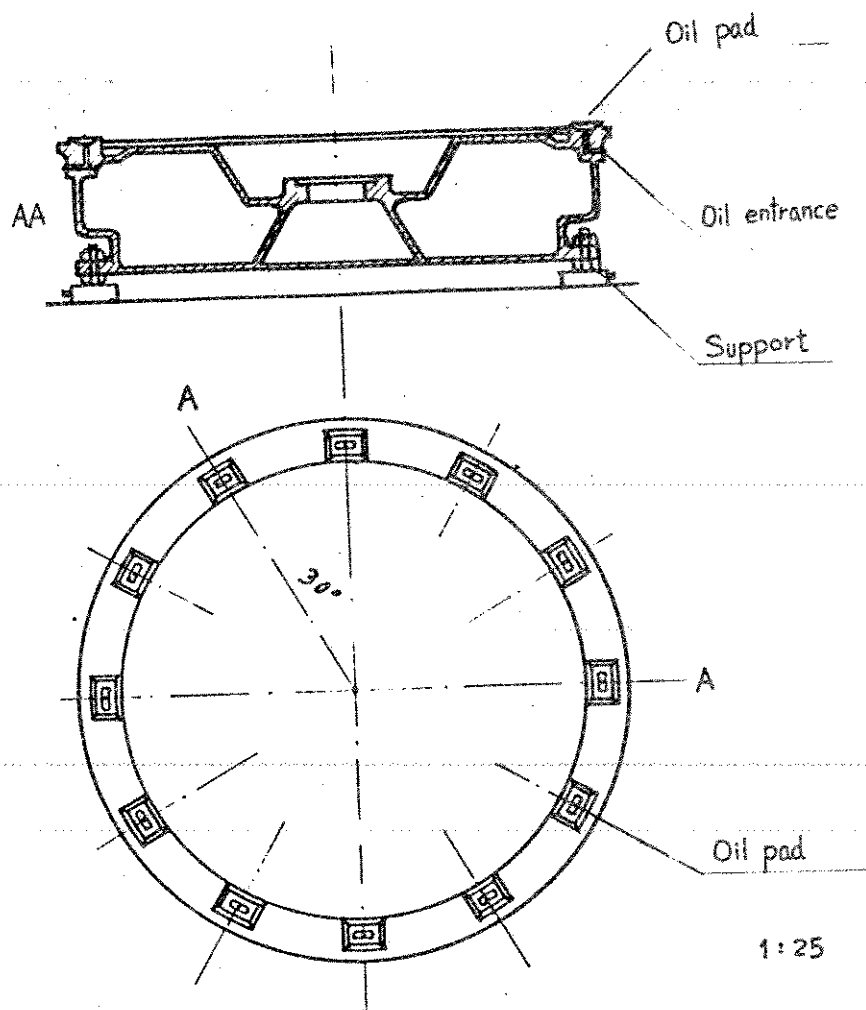just right to the twelve oil pads of the revolving stage(Fig2).

Fig.2. The twelve pads of the hydrostatic oil bearing

As for the second and fourth harmonics, they all originate from the deviation of the azimuth axis caused by the coupling of the drive roll with the rubbing disc(Fig.3). The drive roll is located at one side of the mount and its influence upon the azimuth axis may be regarded as the superimposition of both of the rigid and flexible compositions. The rigid composition influences the first harmonic and the flexible one produces the second and fourth harmonics. This analysis has been proved by the experiments. When the coupling of the driving roll with the rubbing disc is released, the second and fourth harmonics would nearly disappear and the first harmonic would have an obvious change. In addition, it is also found that both of the amplitude and phase of the first harmonic will have a slow and smooth change owing to the effects of the weather on the concrete pier,on which rests the mount. On the contrary, no notable variations would happen in the components, such as the third and twelveth harmonics,etc.,which express the internal properties of the azimuth axis. It is necessary to note that a time-dependent linear term is included in the results, although its value
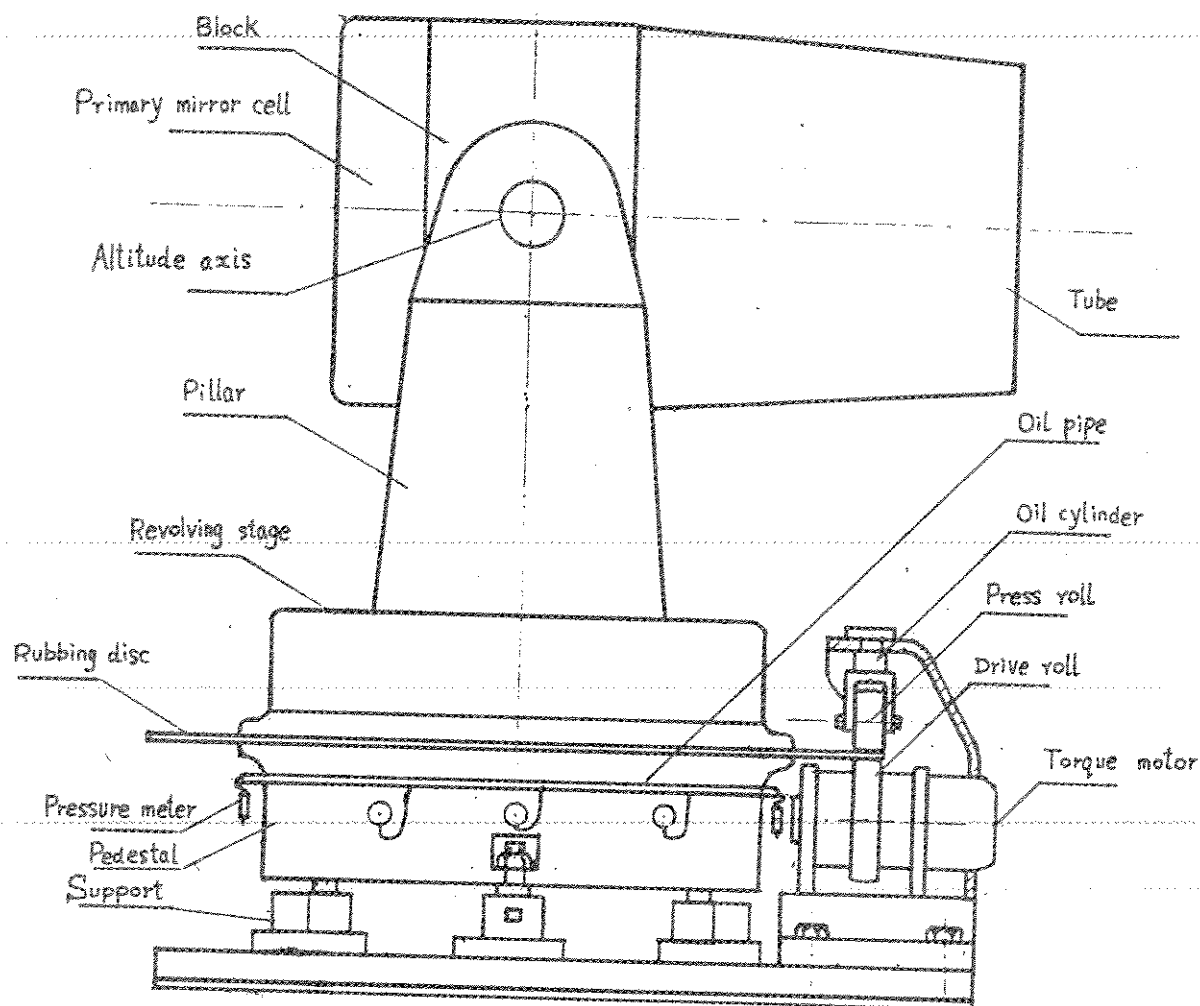
Block

Primary mirror cell

Altitude axis

Tube

Pillar

Oil pipe

Oil cylinder

Revolving stage

Press roll

Drive roll

Rubbing disc

Torque motor

Pressure meter

Pedestal

Support

Fig. 3 . Azimuth axle drive assembly and its effects on the azimuth axis

1 : 25

is very small. The reason why there exists the linear term
is that the measured value at 0° point at the beginning of the
measurement may not be in accordance with that at the end of
the measurement after running a circle. But if the measure-
ment is repeatedly made at the 0° point in a short period,
the measured values tally well with each other. Only in a
rather long time interval when the measurement at the same
point is made, the level bubble can shift in the same direc-
tion. It is considered that the reason why this phenomenon
appears is that a substitute is used as the support of the
bubble, of which the structure at either end is extremely
unsymmetric. Even if there is no temperature gradient in the
surrounding environment, the bubble will shift in the same
direction owing to the time-dependent variation in the tempe-
rature within the dome. Therefore, it is reasonable to intro-
duce the linear term to the measured results. It does not
represent the internal characteristics of the axis, but shows
that there is a linear variable term in the data, caused by
the effects of the external environment on the measuring
device.

Finally, the following formula is adopted to fit the measured data.

$$Y = a_1 \cos x + b_1 \sin x + a_2 \cos 2x + b_2 \sin 2x +$$
$$+ a_3 \cos 3x + b_3 \sin 3x + a_4 \cos 4x + b_4 \sin 4x + \qquad (1)$$
$$+ a_{12} \cos 12x + b_{12} \sin 12x + kx + c$$

For the data of every circle (the 37 measured values are expressed by Y_i), the twelve coefficients awaiting determination in the above equation can be calculated by the least square method. From the residua $\triangle Y_i = Y_i - Y$ and equation(2) the root-mean-square of the fitting error M_f may be obtained, of which the mean is about 0".08.

$$M_f = \sqrt{\sum \triangle Y_i^2 / (37 - 12)} \qquad (2)$$

The R.M.S. of the fitting contains the random wobble of the axis and the measuring error. The quantitative estimation should be made for our measuring method. It is found in the process of the analysis of the measured data that the random wobble of the axis does not happen in some small districts. So in this case the relation between the shift S of the bubble and the rotation angle θ can be determined accurately (Fig.4). The data θ_i, S_i can be fitted by a quadratic curve $S = a \theta^2 + b \theta + c$, which represents the motion model without wobble. The residua $\triangle S_i$ of the measured values S_i with respect to the fitting curve can be used to estimate the measuring accuracy. The R.M.S. error in the measurement is

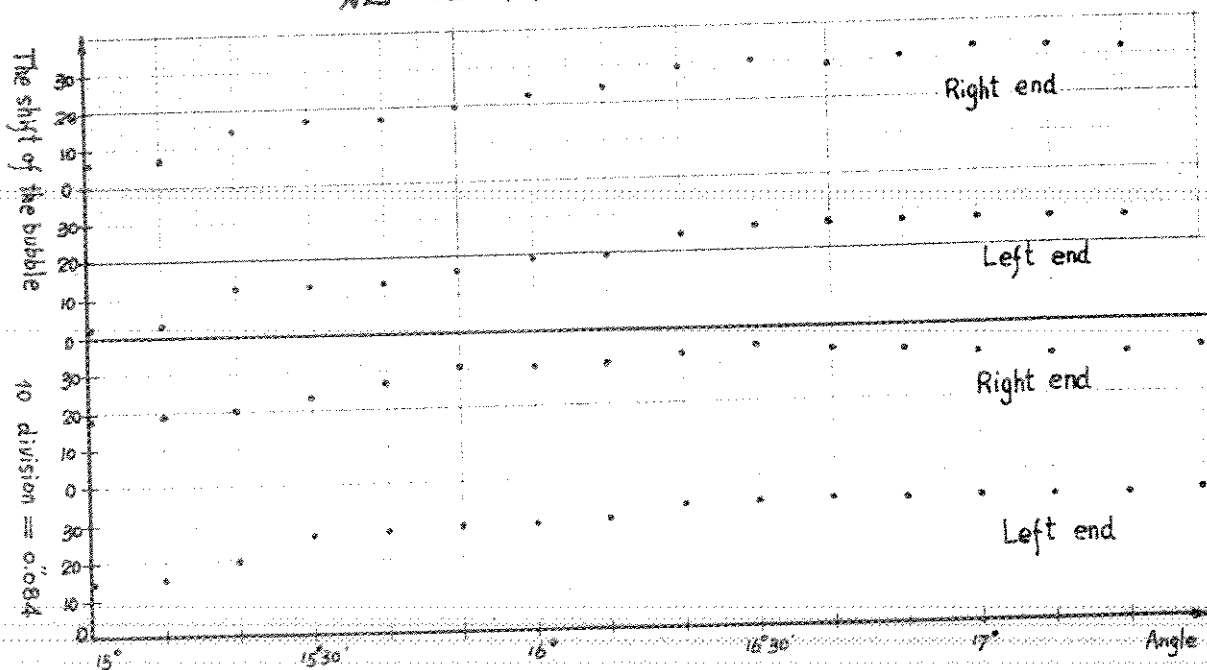$$M_s = \sqrt{\sum \triangle S_i^2 / (N - 3)} \qquad (3)$$

Fig.4 . The relation between the shift of the bubble and rotation angle

where N is the number of the measuring points. A certain district of 3" is chosen where a measurement is made at every

10′. Fig.4 shows two measured results. The repeatability of two measurements is very good and the root-mean-square error of the measurement is 0″.015. Therefore, the values obtained from formula(2) primarily are the random wobble of the axis.

The data of 20 circles are listed in Table 1 and Table 2, where Ai represents the amplitude of the ith harmonic.

IV. Conclusions

(1) It can be seen from the data listed in Table1 and Table2 that the r.m.s. errors calculated from the measured data of every circle are quite approximate to one another. The standard deviation is used to express their dispersion, of which the value is about 0″.01, being equivalent to the measuring error. It is shown that the tested result for the wobble of the azimuth axis is reliable.

(2) The systematic error model measured in a direction is different from that in the direction perpendicular to the former one. It is shown that a rigid model can not be used to describe the wobble of the axis. Hereafter, the correction for the telescope pointing must be made separately according to the results measured in the two directions.

(3) The first harmonic is affected by the influence of the environment on the concrete pier, but the other harmonics mainly have relation to the structure of the mount, and therefore they are all relatively stable. From now on, the first harmonic will be determined by the monitor of the relation between the first harmonic and the environments or by the observation of stars. Then the effect of the wobble of the azimuth axis on the telescope will be limited within the range approximate to that of the wobble of the azimuth axis stated in this paper. This is undoubtedly advantageous to the realization of the lunar laser ranging by means of the absolute pointing.

Unit: arc second

N	A_1	A_2	A_3	A_4	A_{12}	M_f
1	0.432	0.174	0.218	0.087	0.226	0.066
2	0.681	0.232	0.237	0.071	0.211	0.069
3	0.664	0.154	0.273	0.101	0.221	0.064
4	0.921	0.229	0.265	0.127	0.261	0.081
5	0.869	0.194	0.276	0.102	0.238	0.082
6	0.740	0.207	0.247	0.108	0.233	0.078
7	0.705	0.175	0.232	0.089	0.212	0.068
8	0.743	0.176	0.209	0.084	0.206	0.080
9	0.665	0.171	0.221	0.105	0.257	0.095
10	0.730	0.192	0.246	0.106	0.238	0.078
mean	0.715	0.190	0.242	0.098	0.230	0.076
σ_x	0.124	0.024	0.022	0.015	0.018	0.009

Table1 The bubble is parallel with the altitude axis.

Unit: arc second

N	A_1	A_2	A_3	A_4	A_{12}	M_f
1	2.014	0.478	0.203	0.086	0.159	0.094
2	2.046	0.470	0.209	0.080	0.161	0.091
3	2.056	0.465	0.228	0.095	0.140	0.096
4	2.235	0.462	0.259	0.137	0.146	0.077
5	2.338	0.481	0.222	0.124	0.150	0.074
6	2.323	0.463	0.212	0.119	0.131	0.059
7	2.265	0.482	0.245	0.123	0.143	0.074
8	2.159	0.466	0.233	0.111	0.143	0.063
9	2.190	0.499	0.243	0.122	0.176	0.075
10	2.141	0.475	0.245	0.124	0.155	0.064
mean	2.177	0.474	0.230	0.112	0.150	0.077
σ_x	0.109	0.011	0.017	0.018	0.012	0.012

Table2 The bubble is perpendicular to the altitude axis.

DOUBLE PEAK POLARIZED INTERFERENCE FILTERS

M.L. White
Lure Observatory
Institute for Astronomy
University of Hawaii
Kula, HI 96790

Telephone (808) 878-1215
Telex 7238459

ABSTRACT

A new type of high transmission, narrow bandpass filter is tested at the University of Hawaii's Lunar Laser Ranging Observatory. In this article, the Daystar double peak, polarized interference filter is described. The filter performance is characterized through the evaluation of several tests.

DOUBLE PEAK POLARIZED INTERFERENCE FILTERS

I. Introduction

The Daystar double peak interference filter utilizes a solid spacer birefringent etalon. The etalon is cut to a half wave thickness and the refractive index of the etalon material is such that both orthogonal transmission modes are supported. This results in the transmission of both the vertical and horizontal light components at a desired wavelength. A single peak filter of the same type would pass only one polarization component resulting in a 50% loss of transmission at the desired wavelength. Finding birefringent material of acceptable quality and cutting the material at perfect half-wave plate thicknesses are the major limiting factors in the construction of double peak filters. Therefore, sources for these filters are limited.

Following are specifications for the filter described in this paper:

Transmission Wavelength: 532 Nanometers

Bandwidth: 1.0 Angstrom FWHM +/- 0.2 angstrom

Transmission: 28% per channel (This gives an actual throughput for
our application of 28%)

Blocking: Full short side to x-ray optical density = 6.0
Long side to 900 nanometers optical density = 5.0

Clear Aperture: 32 mm.

Filter components: Instrument quality, 60-40 scratch dig. Anti-reflection coated air/glass interfaces for minimum of 0.2 % reflectance. Installed in a temperature regulated oven providing +/- .05 angstrom on band control and minimum +/- 1.0 angstrom off-band search capability.

II. Test Results

The filter was first tested on the University of Hawaii's, Mees Observatory solar spectrograph. The digitized signal from a silicon vidicon tube was used to measure the transmitted light through the filter and then without the filter. A graph was then plotted comparing the amount of light transmitted at 532 nanometers with no filter in place with the amount of light transmitted at 532 nanometers with the filter in place. The filter transmission was measured to be 28% with a FWHM bandpass of 1 angstrom (figure 1). At this time it was noted that the recommended on band temperature setting was not correct. In order to tune the filter on band, the recommended temperature had to be raised approximately 3 degrees centigrade to achieve maximum transmission at 532 nanometers. This was easily accomplished with the adjustable temperature controller, although the controller was near its maximum setting. The manufacturer doubted that the temperature calibration performed at the factory was nearly one angstrom off. However, the additional

tests performed also indicated that to achieve optimum transmission the filter temperature had to be raised.

The filter was then placed in the station's satellite calibration receive package. The average return signal off of the calibration target board was measured with a receive energy monitor through the filter and then without the filter in line with the detector. The comparisons of these two sets of data revealed that about 75% less energy was received with the filter in line with the detector than was received when the filter was not in line. This test was more subjective than the first and had an error factor of approximately plus or minus 10%.

Finally, the filter was tested during actual lunar ranging. The histograms in figures 2 and 3 show the number of photo-electron events obtained during several runs. It is difficult to apply a transmission efficiency number to the results, since one can only compare the data to other ranging data taken on nights when seeing conditions might be considerably different. A test of this nature is greatly affected by seeing conditions and equipment performance on a given night. However, when comparisons are made with lunar data taken with a four angstrom filter with a transmission of about 40%, the data rate is within expectation.

III. Test Considerations

Angle of Incident Energy and Effects of Temperature Variance

Particular emphasis was placed on controlling the angle of incidence during these tests. When a narrow bandpass filter is tilted from the normal, the pass band will broaden while shifting its center to the shorter wavelengths. When testing the filter on the solar spectragraph a real-time display was monitored while the filter tilt was adjusted for maximum red shift.

Increasing the filter's correct operating temperature will shift the bandpass towards the longer wavelengths. Likewise, decreasing the filter's normal room temperature will shift the band pass toward the shorter wavelengths. The change in bandpass as a function of temperature depends on the spectral location of the filter and falls within a range of .15 to .4 angstrom per degree centigrade change. The Daystar 1 angstrom filter is installed in a temperature regulated oven providing +/- .05 angstom on band control with a maximum +/- 1.0 angstom off band search capability.

IV. Conclusions

The filter performed at a level of efficiency consistent with the manufacturer's specifications with the exception of the discrepancy noted with the temperature controller. Daystar originally agreed to provide a filter with a throughput of 25%. The completed filter, however, was measured to have a throughput of 28%. This is an excellent overall transmission for a 1 angstrom bandpass filter and it should be useful to any lunar ranging station desiring to improve the receiver, signal-to-noise ratio. The problem with the temperature controller should lead future users of this filter type to verify on-band tuning since any deviation from the filter's correct operating temperature will lead to a significant change in the bandpass.

The filter was originally expected to increase the station's coverage through the maximum lunar illumination period. However, when the filter was tested during several full moon periods, a significant improvement in the signal to noise ratio was not observed. The background noise was considerably reduced as expected however, very few lunar events were observed. It is possible that more attempts at full moon ranging are needed to verify this result. More recently, other lunar stations have reported limited ranging success

during full moon that cannot be entirely related to increased lunar noise during full moon. This has led to some speculation that the Apollo reflectors lose some efficiency as they heat up during maximum lunar illumination.

Recently, the LURE Observatory achieved its first daylight lunar ranges. As a consequence normal lunar operations will be extended into daylight hours. More testing of the 1 angstrom double peak filter will be conducted during daylight hours where a significant improvement in the signal to noise ratio can be expected.
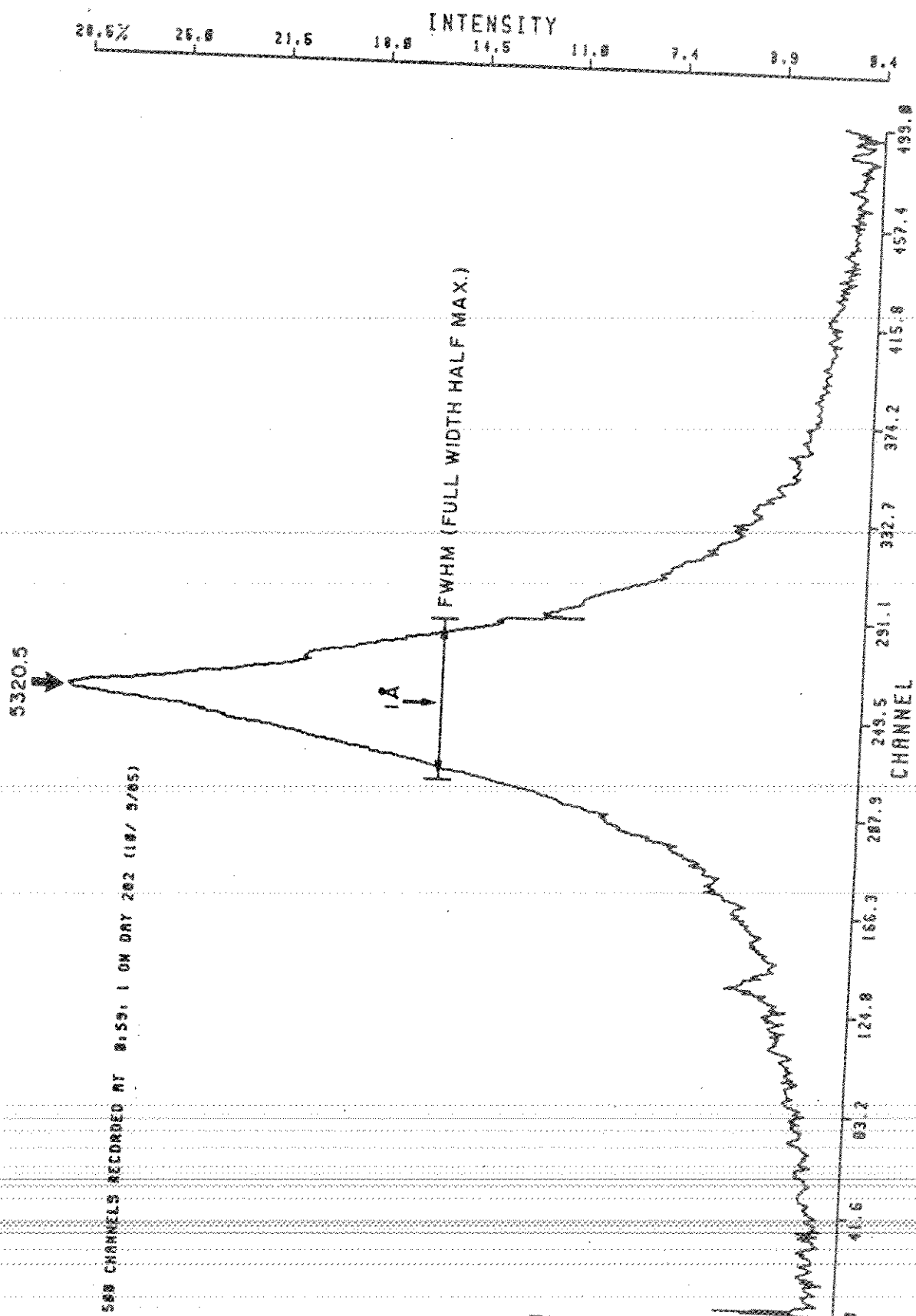
V. Acknowledgments

FIGURE 1

HISTP(8.30)
Data histogram for Input File : LUN31210.279
LUNAR Data Histogram
   460 DATA RECORDS WITH   560 RANGES

```
    Less than     50.0000   211 !*******************************************************
  50.0000 TO      52.0000     3 !***
  52.0000 TO      54.0000     2 !**
  54.0000 TO      56.0000     3 !***
  56.0000 TO      58.0000     2 !**
  58.0000 TO      60.0000     1 !*
  60.0000 TO      62.0000     1 !*
  62.0000 TO      64.0000     3 !***
  64.0000 TO      66.0000     7 !*******
  66.0000 TO      68.0000     2 !**
  68.0000 TO      70.0000     4 !****
  70.0000 TO      72.0000     4 !****
  72.0000 TO      74.0000     5 !*****
  74.0000 TO      76.0000     5 !*****
  76.0000 TO      78.0000     4 !****
  78.0000 TO      80.0000     7 !*******
  80.0000 TO      82.0000     2 !**
  82.0000 TO      84.0000     3 !***
  84.0000 TO      86.0000    30 !******************************
  86.0000 TO      88.0000    31 !*******************************
  88.0000 TO      90.0000     2 !**
  90.0000 TO      92.0000     3 !***
  92.0000 TO      94.0000     0 !
  94.0000 TO      96.0000     0 !
  96.0000 TO      98.0000     3 !***
  98.0000 TO     100.0000     3 !***
 100.0000 TO     102.0000     4 !****
 102.0000 TO     104.0000     0 !
 104.0000 TO     106.0000     3 !***
 106.0000 TO     108.0000     4 !****
 108.0000 TO     110.0000     3 !***
 110.0000 TO     112.0000     3 !***
 112.0000 TO     114.0000     1 !*
 114.0000 TO     116.0000     0 !
 116.0000 TO     118.0000     1 !*
 118.0000 TO     120.0000     1 !*
 120.0000 TO     122.0000     2 !**
 122.0000 TO     124.0000     2 !**
 124.0000 TO     126.0000     2 !**
 126.0000 TO     128.0000     2 !**
 128.0000 TO     130.0000     1 !*
 130.0000 TO     132.0000     4 !****
 132.0000 TO     134.0000     4 !****
 134.0000 TO     136.0000     0 !
 136.0000 TO     138.0000     4 !****
 138.0000 TO     140.0000     4 !****
 140.0000 TO     142.0000     2 !**
 142.0000 TO     144.0000     1 !*
 144.0000 TO     146.0000     2 !**
 146.0000 TO     148.0000     4 !****
 148.0000 TO     150.0000     2 !**
    More than    150.0000   163 !*************************************************
```
A TOTAL OF   560 DATA POINTS PROCESSED

APOLLO 15
OCTOBER 6, 1985 2:10 A.M.
20 MINUTE RUN
1Å 30^m

FIGURE 2

```
HISTP(8.30)
Data histogram for Input File : LUN01236.279
LUNAR Data Histogram
    40 DATA RECORDS WITH      43 RANGES
    Less than      50.0000      6 !******
  50.0000 TO      52.0000      0 !
  52.0000 TO      54.0000      0 !
  54.0000 TO      56.0000      0 !
  56.0000 TO      58.0000      0 !
  58.0000 TO      60.0000      0 !
  60.0000 TO      62.0000      0 !
  62.0000 TO      64.0000      0 !
  64.0000 TO      66.0000      0 !
  66.0000 TO      68.0000      0 !
  68.0000 TO      70.0000      0 !
  70.0000 TO      72.0000      0 !
  72.0000 TO      74.0000      0 !
  74.0000 TO      76.0000      1 !*
  76.0000 TO      78.0000      0 !
  78.0000 TO      80.0000      0 !
  80.0000 TO      82.0000      0 !
  82.0000 TO      84.0000      0 !
  84.0000 TO      86.0000      1 !*
  86.0000 TO      88.0000      5 !*****
  88.0000 TO      90.0000      5 !*****
  90.0000 TO      92.0000      0 !
  92.0000 TO      94.0000      0 !
  94.0000 TO      96.0000      0 !
  96.0000 TO      98.0000      0 !
  98.0000 TO     100.0000      0 !
 100.0000 TO     102.0000      0 !
 102.0000 TO     104.0000      0 !
 104.0000 TO     106.0000      0 !
 106.0000 TO     108.0000      1 !*
 108.0000 TO     110.0000      0 !
 110.0000 TO     112.0000      1 !*
 112.0000 TO     114.0000      1 !*
 114.0000 TO     116.0000      1 !*
 116.0000 TO     118.0000      0 !
 118.0000 TO     120.0000      0 !
 120.0000 TO     122.0000      0 !
 122.0000 TO     124.0000      0 !
 124.0000 TO     126.0000      0 !
 126.0000 TO     128.0000      1 !*
 128.0000 TO     130.0000      2 !**
 130.0000 TO     132.0000      0 !
 132.0000 TO     134.0000      0 !
 134.0000 TO     136.0000      0 !
 136.0000 TO     138.0000      0 !
 138.0000 TO     140.0000      0 !
 140.0000 TO     142.0000      0 !
 142.0000 TO     144.0000      0 !
 144.0000 TO     146.0000      0 !
 146.0000 TO     148.0000      0 !
 148.0000 TO     150.0000      1 !*
    More than   150.0000     17 !*****************
A TOTAL OF     43 DATA POINTS PROCESSED.
```

APOLLO II
OCTOBER 6, 1985 2:36 A.M.
20 MINUTE RUN
1Å 30^m

FIGURE 3

FILTER ADVANTAGES

- GOOD TRANSMISSION, 28%, FULLY BLOCKED.

- DURABLE. (Survived Sounding Rocket Crash).

- COMPACT. (2" x 3")

- EASY TO CONTROL TEMPERATURE.

- SINGLE PASS BAND.

- WORKS IN SYSTEMS AS FAST AS f/20.

- REASONABLE COST ~ $3,000.00 U.S.

FILTER DISADVANTAGES

- LIMITED NUMBER OF VENDORS AVAILABLE.

- DIFFICULT TO MANUFACTURE.

- SENSITIVE TO >1° DEVIATION FROM NORMAL.

FIGURE 4

EFFECTS OF TELESCOPE DESIGN ON LASER BEAM POINTING ACCURACY

R. Korakitis
Department of Topography
National Technical University of Athens
Heroon Polytechniou 9
GR-157 73 Zografos - Greece -

Telephone (01) 777 3613
Telex 215032 GEO GR

ABSTRACT

This work presents some studies about the effects of the optical design of the telescope on the beam pointing accuracy of the SLR system at Dionysos Satellite Geodesy Observatory.

A brief description of telescope and mount is given, with emphasis on components critical to beam alignement. Possible torsional flexure of the horizontal axis is examined and is found to be unimportant.

The path of the laser beam through the mount is softwaremodelled and beam deviations upon exit are computed for different positions of adjustable optical components. At the same time, it is shown that precession of the beam, due to improper alignement, has pratically no effect on the optical path length, so no system delay changes are expected for different orientations of the mount. This prediction is experimentally confirmed down to the performance limit of the system (about 2 cm).

1. Introduction

This work reports some results of studies, conducted at Dionysos Satellite Geodesy Observatory, concerning the mechanical and optical performance of the mount and telescope used in the Satellite Laser Ranging system. The purpose of the studies is to establish the accuracy limit of the system with regard to laser beam pointing and system delay stability, since the mount was originally designed to be used with a 1st generation Ruby laser, having much lower precision capabilities.

In the first part, a brief description of mount and telescope is given, indicating components critical to mechanical and optical adjustments. A possible torsional flexure of the horizontal axis is examined both theoretically and experimentally and is found to be unimportant.

The second part describes the laser beam path and its software model. In this model, all optical components are suitably represented and ray-tracing results show how each individual adjustment affects the alignement of the beam and the optical path length. For all reasonable values of beam deviation, the path length does not depend on the orientation of the mount. The last section of the work describes the experimental verification of this prediction, through system delay measurements at various orientations.

2. Characteristics of the mount

The SLR system at Dionysos uses a conventional altitude over azimuth design, with separate transmit and receive optics and a coude optical path. The overall lay-out of the mount and telescope is shown in Fig.1.

Both rotation axes are realized by pairs of conical roller bearings and their exact orientation can be adjusted by suitably located screws. A precision level permits alignement of the primary (azimuth) axis within 3 arcsec of the local vertical. Similarily, the tilt of the secondary (altitude) axis is adjustable to within 3 arcsec of the horizontal plane. In addition to the roller bearings, the altitude axis is supported by preloaded bronze bushings, in order to minimize flexure. Rotation angles of the axes are read by optical encoders, which have a resolution of 1 millidegree and are situated by the respective drive gears. The rotation of the axes is accomplished by step-motors having a resolution of $0°.001$ per step and repeatability 1 millidegree (RMS). Therefore, the positioning accuracy of the mount is limited to about 5 arcsec.

With regard to the distribution of masses, one should note that the center of mass (CM) of the receiving telescope lies behind the altitude axis (when the telescope is in the horizontal plane), whereas the CM of the transmitter lies in front of the axis. Since the corresponding moments have opposite direction, the altitude axis is rotationally balanced. However, these moments can cause a torsional flexure of the steel tube that realizes the axis. The rotation angle of this axis (i.e. the altitude) is determined at the transmitting end of the tube, where the altitude drive and the encoders are situated, so any torsional flexure will show itself as a vertical deflection of the receiving telescope. A rough estimate of the magnitude of this deflection can be made using elementary elasticity theory [1]:

To a first approximation, the deflection angle ϕ due to torsional flexure of a thin cylindrical tube is given by:
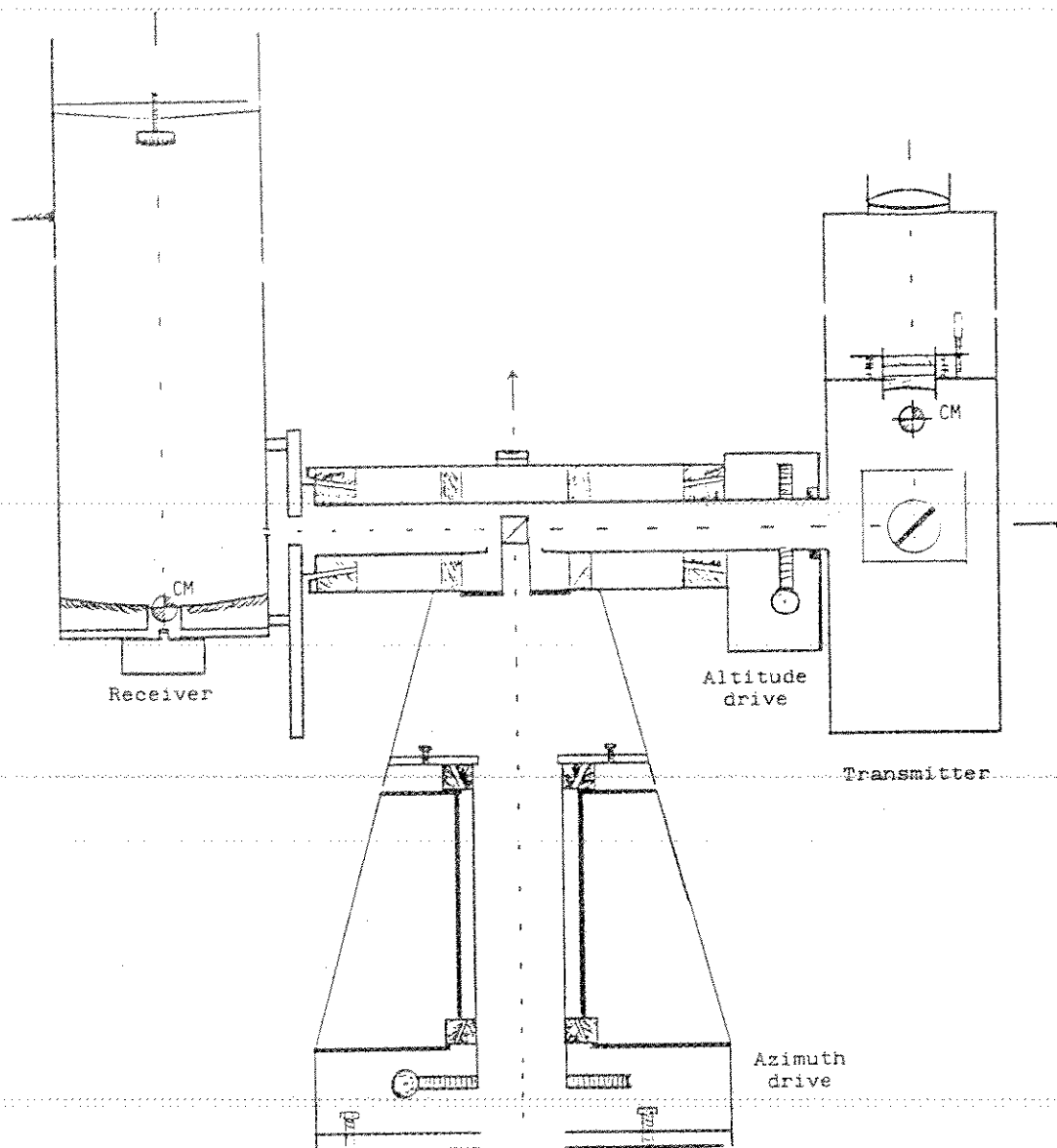
$$\phi = \frac{M \cdot l}{G \cdot r^2 \cdot s}$$

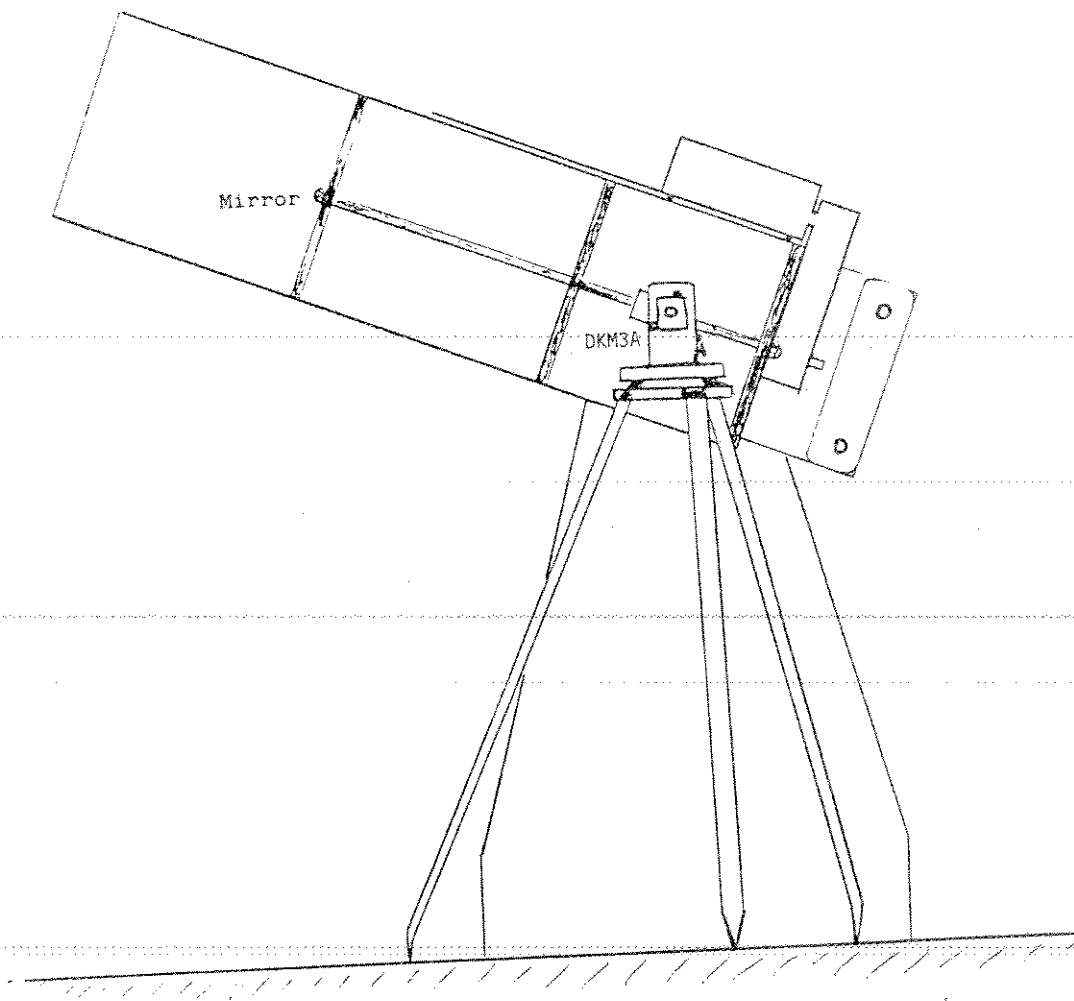Fig. 1 : Mechanical lay-out of mount and telescopes

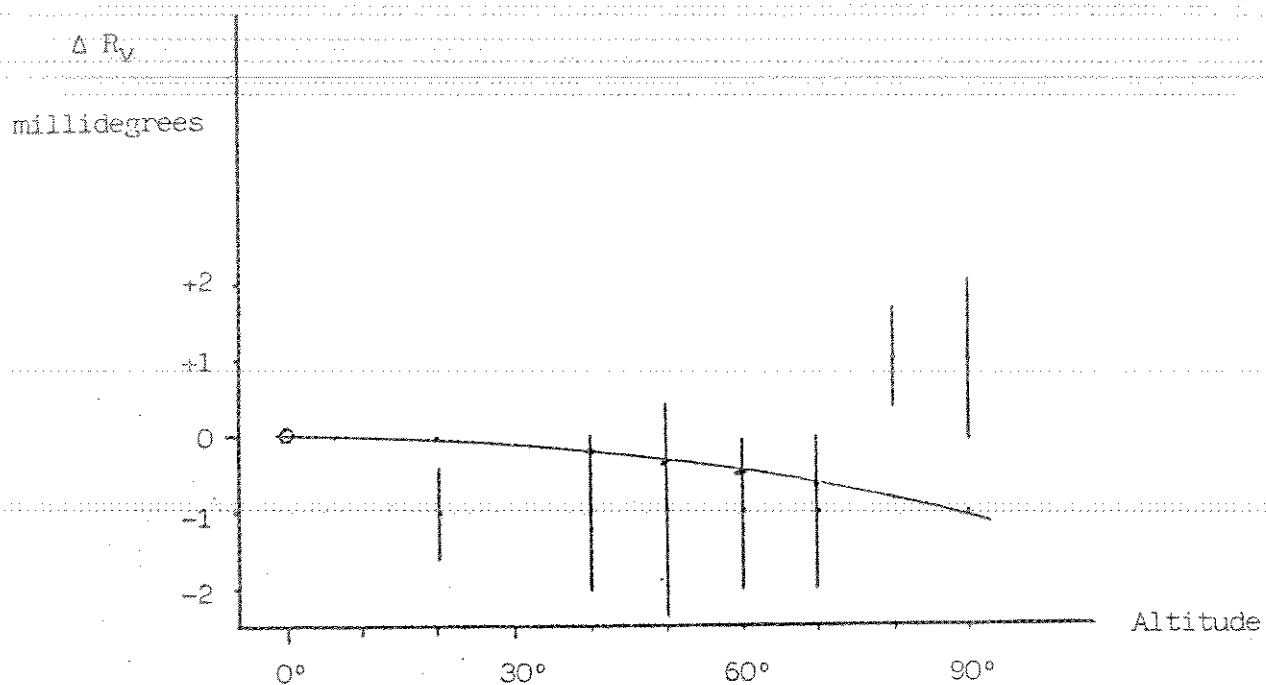Fig. 2 : Set-up for the torsional flexure experiment

Fig. 3. Vertical reading differences (theodolite-telescope)
vs. altitude. ΔR_V defined to be zero at $v = 0°$.

The solid curve shows the effect of the expected
torsional flexure.

where the symbols and their values for this particular case are:

M = the applied torque = 100 kgr* × 20 cm × cosv
l = the length of the tube = 100 cm
G = the shear modulus of the material = 8×10^5 kgr* cm^{-2}
r = the radius of the tube = 10 cm
S = the cross-section of the tube = 157 cm^2

Therefore, the maximum deflection (at altitude v=0°) is about 16 microradians or 0°.001. Since the predicted value of the deflection is similar to the positioning accuracy of the axis, torsional flexure is considered to be unimportant. In any case, an experimental check was performed as follows:

A small mirror was fixed on the outside wall of the receiving telescope, perpendicular to the optical axis. A precision theodolite, type Kern DKM3A, was placed by the receiver so that its horizontal axis roughly coincided with the altitude axis of the mount (Fig.2). The theodolite was used as an autocollimator, projecting the image of an illuminated crosshair to the mirror. In this way a direction, approximating the optical axis, was realized that remained fixed with regard to the receiver. The altitude of the telescope was varied and the encoder readings were compared with the corresponding readings of the vertical angle of the theodolite. Two independent series of such measurements were taken and the mean values of the differences are shown in Fig.3, along with the expected value of the deflection. No systematic deviation that can be attributed to torsional flexure is evident. The deviation of the measurements near the zenith, currently under further investigation, is probably connected with the behaviour of the anti-backlash torque motors of the altitude drive.

3. The laser beam path model

A general schematic of the laser beam path is shown in Fig 4. Upon exit from the laser unit, the beam is twice deflected through 90° by dichroic mirrors that separate the 532nm radiation from the IR. The laser beam, after expansion, is directed to the 1st mirror of the coude path that sends it upwards, along the vertical (azimuth) axis of the mount.

In order to facilitate the alignement of the beam, an auxilliary optical setup is under construction by the vertical axis. It mainly consists of an autocollimator and a fixed mirror, that will realize a permanent reference direction for the laser beam. A sample of the laser beam will be brought into this path by inserting a pellicle beam-splitter. At the same time, this setup will permit direct viewing through the transmitting telescope, enabling thus a direct check of the pointing of the telescope using observations of stars.

The alignement procedure consists of three main parts:

a. Adjustment of the last dichroic mirror, together with expander, for pitch, yaw and linear position. Then, adjustment of the 1st coude mirror for pitch, yaw and transverse linear position so that the beam exactly follows the azimuth axis of the mount.

b. Adjustment of the 2nd coude mirror, which actually is a right-angle prism situated at the intersection of the axes, for pitch, yaw and linear position so that the beam follows the altitude axis.

When these adjustments are completed, the laser beam should not precess when the mount is rotated to different orientations. At present, that can be achieved within 15 arcsec but this figure is expected to decrease using the alignement setup described earlier.
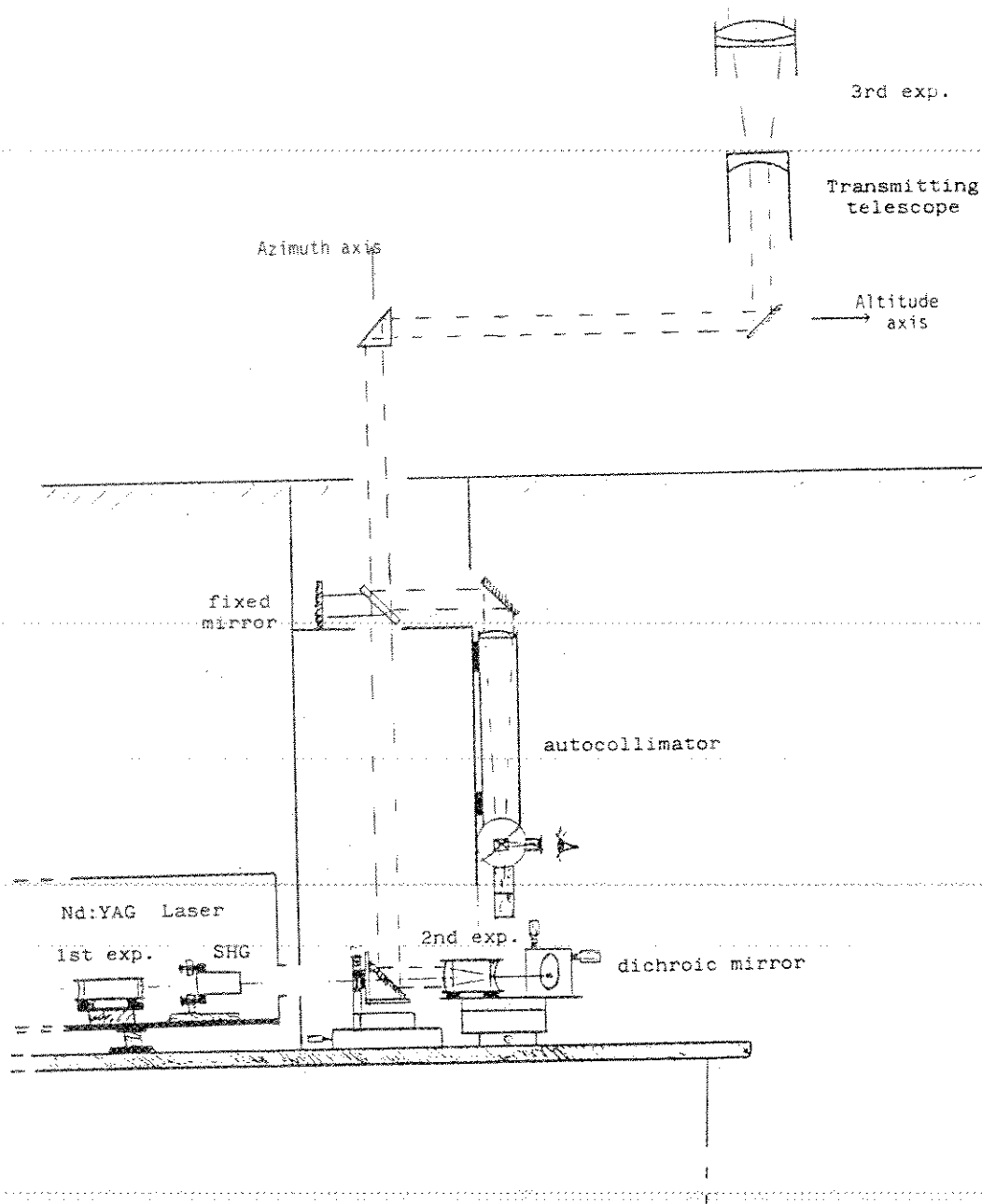
3rd exp.

Transmitting
telescope

Azimuth axis

Altitude
axis

fixed
mirror

autocollimator

Nd:YAG Laser

1st exp.   SHG

2nd exp.

dichroic mirror

Fig. 4 : Schematic of the laser beam path

c.   The last step involves the adjustment of the 3rd coude mirror, located inside the transmitter, in order to bring the exit laser beam into alignement with the pointing direction of the mount (common direction of transmitter and receiver optical axes). In addition, the final beam expander adjusts the full angle divergence of the beam in the range 10 to 100 arcsec.

Referring to Fig.1, one should note the internal calibration path that is established inside the receiver end of the altitude axis. A very small drop of clear glue, at the hypotenuse face of the central coude prism, scatters some radiation towards the receiver. There, a small prism deflects it towards the main mirror so that it can be acquired by the detection package.

In order to study quantitatively the effects of the several adjustments needed for the alignement of the beam, the optical path was modelled in the computer. This software model analytically treats the deflections of the beam at all mirrors and prisms in the path, the position and orientation of which can be varied in accordance with the degrees of freedom of the actual components. The starting point and initial direction of the laser beam, as it leaves the 2nd expander, is taken into account, as well as the distances between the components, which were measured using a Chesterman stainless-steel tape.

The computations are performed using matrix representations of vectors in three rectangular coordinate systems: the (X_0,Y_0,Z_0) system remains fixed in space, with Z_0 along the azimuth axis of the mount (local vertical) and Y_0 towards the local astronomical North. The $(X_1,Y_1,Z_1=Z_0)$ system is produced by rotating the previous one around Z_0 through the azimuth angle A; the X_1 axis is along the altitude axis of the mount. Finally, the $(X_2=X_1,Y_2,Z_2)$ system is derived by rotating the previous one around X_1 through the altitude angle v; the Y_2 axis is along the optical axis of the transmitting telescope. The program outputs the direction of the laser beam upon exit, expressing it as an angular deviation from the Y_2 axis towards a certain direction in the (X_2,Z_2) plane. Figures 6 and 7 are typical examples of the output, showing different locii of beam deviations for constant azimuth or altitude and for different adjustments of the components. In addition, the program computes the total path length, from the starting point of the beam up to a fixed plane outside the last lens of the system, where a retroreflector can be actually placed.

At present, the effects of the final beam expander are computed using the paraxial approximation. Since the overall alignement precision will increase with the installation of the auxilliary optics, a revised program is under development that will perform accurate ray-tracing using the exact refraction matrices.

It is worth mentioning that the program also handles the possibility that the two rotation axes of the mount are skew lines. In such case, the beam will rotate around the Y_2 axis without changing its direction, in the paraxial approximation. In reality, though, the direction of the beam may be affected and this problem is another motivation for developing the exact treatment.

It is apparent that a similar program can be used to study any other telescope design as well, provided that all relevant positions and orientation of components are properly introduced.
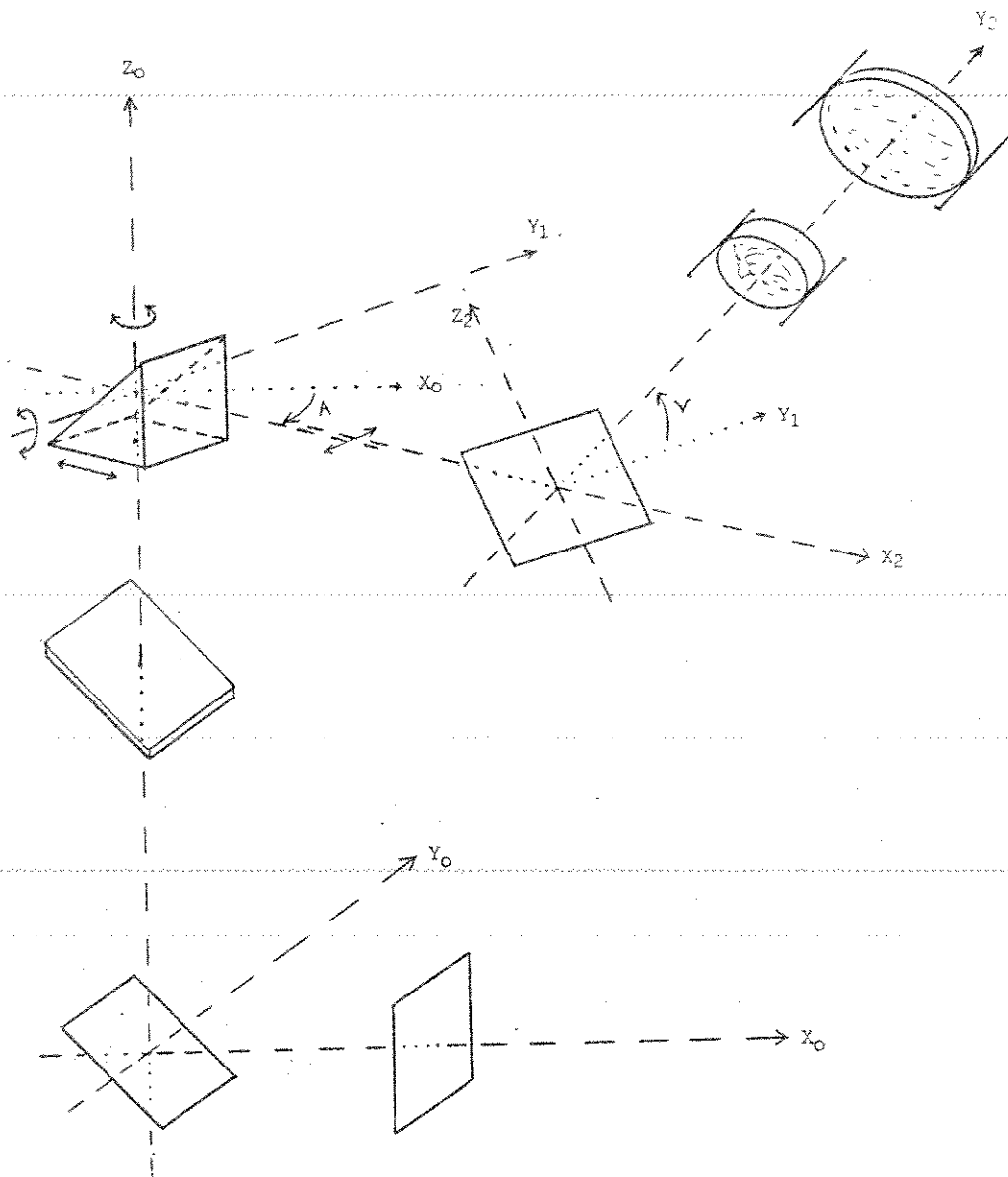
Fig. 5 : Geometry of the laser beam path model

Initial beam tilt : $20''$ to $-Z_0$
Prism displacement: 0 mm
    angular dev. : $-20''$ az
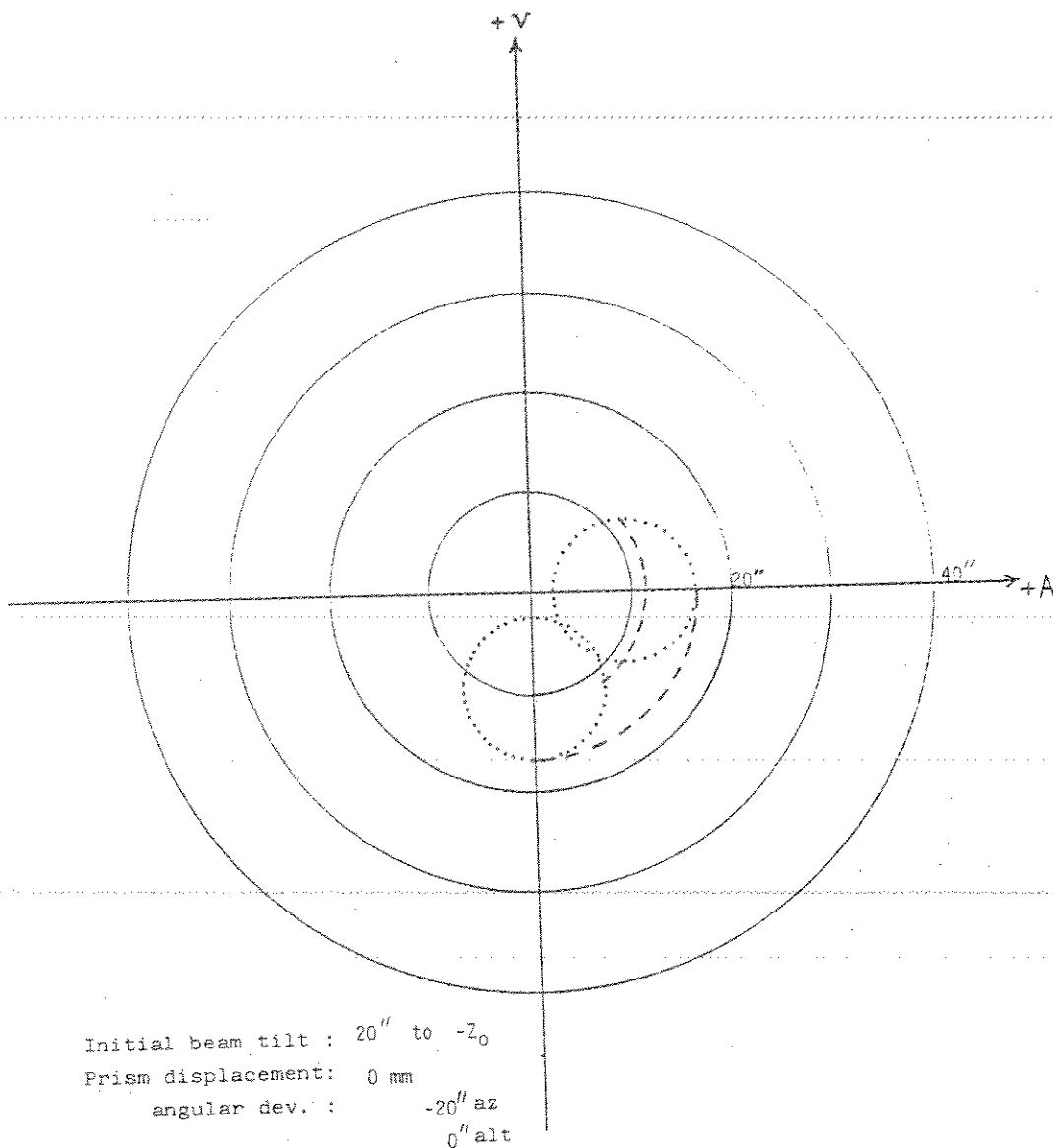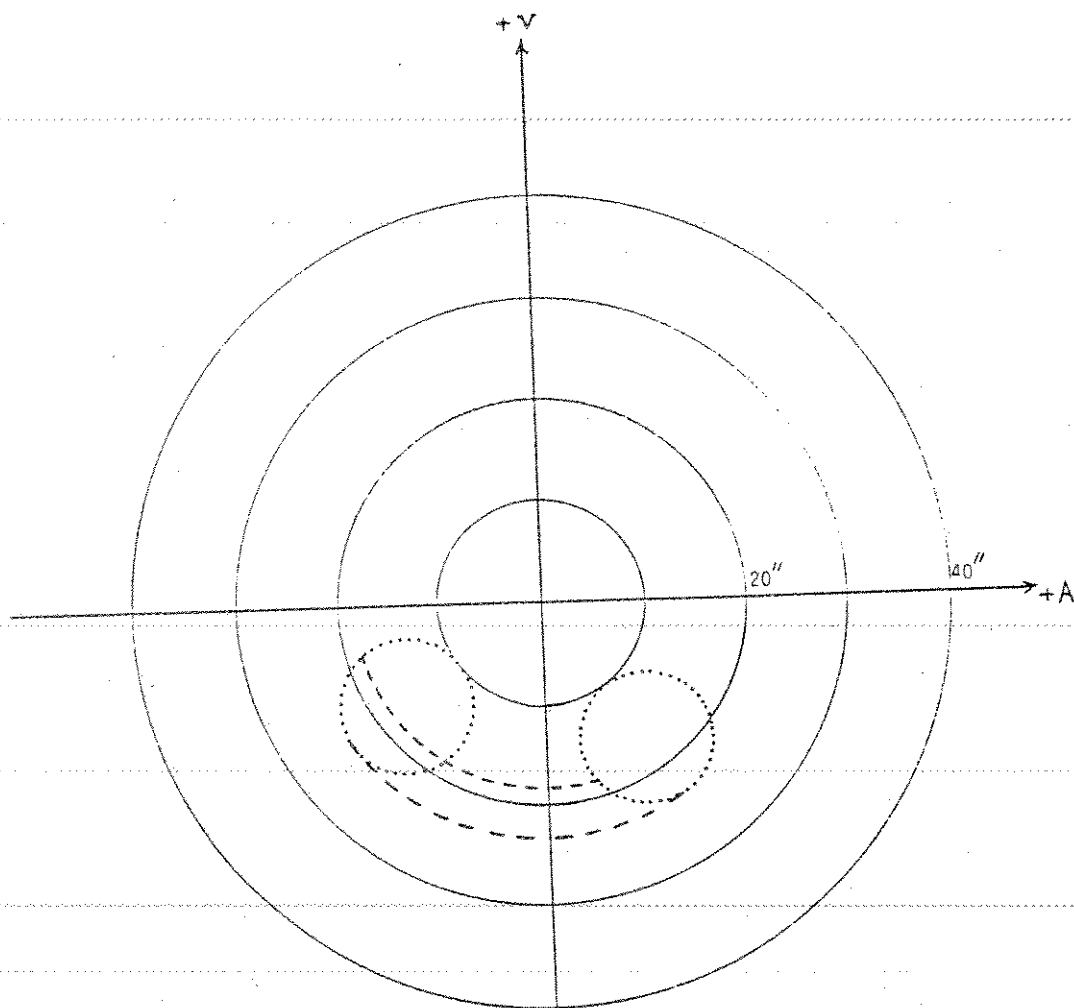 $0''$ alt

Fig. 6 : Laser beam deviation curves
          at constant azimuth (dashed lines)
          and constant altitude (dotted lines)

Initial beam tilt : $10''$ to $-Y_0$ and $18''$ to $-Z_0$
Prism displacement: 0 mm
       angular dev. : $-20''$ az
                          $-20''$ alt
Hor. axis displaced by 1 mm

Fig. 7 : Laser beam deviation curves
         at constant azimuth (dashed lines)
         and constant altitude (dotted lines)

4. System delay measurements

As was mentioned earlier, the software model of the mount includes the total path length of the laser beam, which is directly related to the overall system delay. The computations indicate that the path length is only affected either by a linear displacement of the central coude prism or by the skewness of the two rotation axes. However, for any fixed adjustment of components, the path length is invariant for every orientation of the mount, at least for reasonably small beam deviations (up to several arcminutes!). The implication is that, once the alignement of the beam is even approximately correct, the system delay should not change with orientation of the mount.

This prediction was experimentally tested by measuring the travel time of the laser pulse from a point behind the last dichroic mirror, where a fiber optic link to the START photodiode of the system was placed, to a retroreflector at the transmitter exit and back. The travel time was measured at several different values of azimuth and altitude of the mount and a total of 40 individual measurements were taken in each position. The results are shown in figures 8 and 9 and no variation larger than the resolution of the measurements (about 2 cm [2]) is evident. In addition, one should note that the measurements were taken when the spatial profile of the laser beam was greatly distorted by a damaged SHG crystal. Therefore, a second test is scheduled, to be done after the installation of a new SHG crystal and which will also include a stability check of the internal calibration path.

5. Conclusion

It has been shown that the particular telescope design of the SLR system at Dionysos Observatory presents some problems regarding the alignement of the beam in the coude path, which are studied using a software model of the mount. The results of the study dictate several improvements that can be made to increase the pointing accuracy of the system, with beneficial effects on received energy and return rate. On the other hand, it has been shown, both theoretically and experimentally, that the mount is free from appreciable flexure and is quite immune to system delay (i.e. calibration) changes for different orientations.

I would like to thank Mr. D. Paradissis for his kind help during the flexure test of the telescope.

REFERENCES

1. R.Feynman :"Lectures on Physics" , Addison Wesley Publ. Co. , 1964

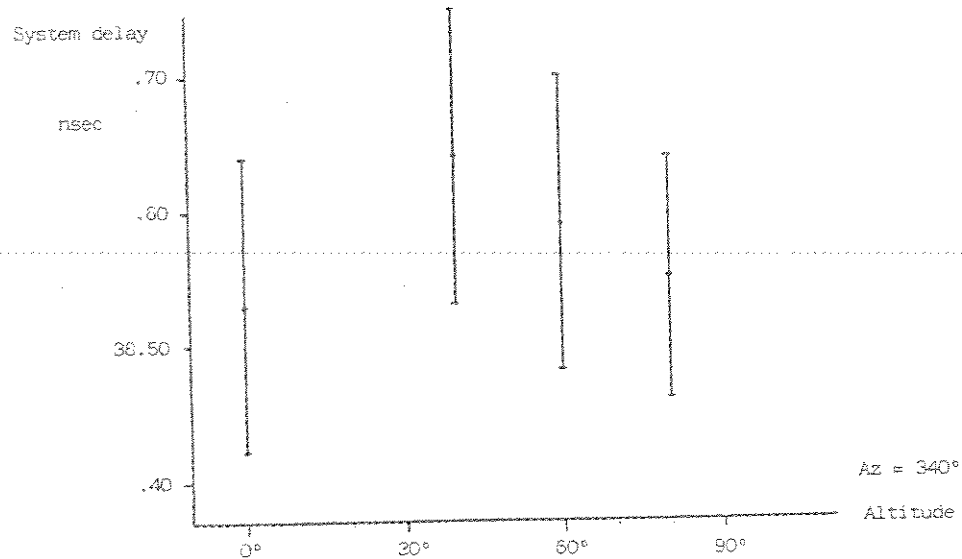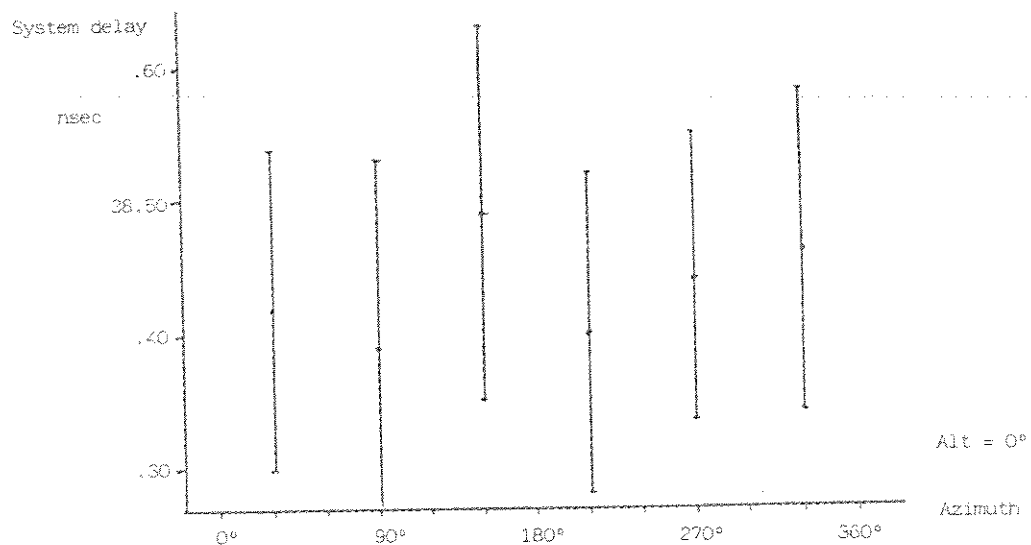2. R.Korakitis :"Performance considerations of the SLR system at Dionysos Observatory", 2nd WEGENER-MEDLAS Conference, Athens, 1986

Fig. 8,9 : System delay measurements